Sedimentology and stable isotope geochemistry of the Trezona Formation; A local or global biogeochemical event?

Robert M. Klaebe

Geology and Geophysics
School of Earth & Environmental Sciences
The University of Adelaide, Australia
Supervisors: Martin Kennedy

Table of Contents

ABSTRACT

High magnitude $\delta^{13}C$ shifts (>12‰) restricted to Neoproterozoic carbonate successions are widely interpreted to reflect a vastly different regime of carbon cycling that changed into the Phanerozoic. Despite isotopic values in the Neoproterozoic being anomalous, they are considered to reflect the $\delta^{13}C$ composition of sea water because the values appear to be reproducible, change systematically, and occur in a similar stratigraphic interval relative to overlying glacial intervals within successions in different basins. The relation to a primary marine origin of the isotopic values in carbonates is key to these isotopic excursions providing constraints on the global carbon mass balance during the Neoproterozoic, that are central to present models of the ancient carbon cycle. The Trezona Formation in the Central Flinders Ranges in South Australia records a large (~9‰) pre-Marinoan glacial $\delta^{13}C$ excursion widely correlated to basins globally and termed the 'Trezona Anomaly'. This study examines the depositional setting of the Trezona Formation using outcrop exposures, petrographic studies, and stable isotope geochemical data and investigates the origin of $\delta^{13}C$ values with respect to lithological and diagenetic controls. $\delta^{13}C$ and $\delta^{18}O$ data was collected using Isotope Ratio Mass Spectrometry. Field observations reported here are inconsistent with an open marine or tidal origin for the Trezona Formation. Sequence boundaries in the form of paleosols and fluvial deposits at the basal and upper contacts respectively indicate that it represents its own discrete depositional cycle. This is contrary to previous interpretations that the Trezona Formation records a broad shallowing upwards trend of widespread marine shales of the underlying Enorama Formation into the overlying glacial sediments of the Elatina Formation. Evidence of frequent desiccation throughout the basal half of the Formation and the limited spatial distribution of the Trezona Formation is suggestive of a consistently shallow, restricted marine or periodically lacustrine depositional setting.

Covariant and diverging relationships between $\delta^{13}C$ and $\delta^{18}O$ values in stratigraphic profiles suggest a lithological relation to isotope values. Furthermore, petrographic data suggests that intervals of the Trezona Formation housing strongly negative $\delta^{13}C$ values (<-5‰) may have undergone digenetic recrystalisation. A diagenetic origin for these values makes them typical of meteorically altered successions in the Phanerozoic, and removes the need for currently popular global biogeochemical models calling for dramatic differences in Precambrian carbon cycling. These observations also imply that the Trezona Formation is not a record homogeneous, open marine $\delta^{13}C$ values and is therefore inappropriate as a correlation of chemostratigraphic events. Rather, it likely records the common alteration of coastal or lacustrine carbonates responding to exposure and alteration during sea-level fall coinciding with the Marinoan glaciation.

Key Words: Trezona, Marinoan glaciation, Carbon Cycling, $\delta^{13}C$, $\delta^{18}O$

INTRODUCTION

Negative $\delta^{13}C$ excursions are widely interpreted to record significant perturbations to the carbon cycle during the Neoproterozoic (Hoffman *et al.* 1998, Schrag *et al.* 2002, Fike *et al.* 2006, Bjerrum & Canfield 2011, Grotzinger *et al.* 2011), with variations of up to 20‰ during the Ediacaran sharply contrasting with the ~5‰ variability observed in the Phanerozoic record (Kennedy *et al.* 2008). Negative $\delta^{13}C$ excursions are poorly time-constrained, but are interpreted to be associated with the Sturtian and Marinoan glaciations, which represent the most severe climatic events recognised in the Earth's history (Halverson *et al.* 2002, Hoffman *et al.* 2002, Tziperman *et al.* 2011). Neoproterozoic post-glacial intervals preserve evidence of the radiation of the earliest multicellular organisms on Earth, suggesting an

intimate relationship between Neoproterozoic glaciation and evolutionary diversity (McFadden *et al.* 2008). Furthermore, the Neoproterozoic carbon-isotope record is constructed based on the correlation of these reproducible isotopic signals in isolated pre-glacial successions globally (Halverson *et al.* 2005). The mechanisms responsible for this isotopic variation remain controversial and are key to understanding the dynamics of the Neoproterozoic carbon cycle (Hoffman *et al.* 1998, Fike *et al.* 2006, Knauth & Kennedy 2009). The implications of isotopic excursions of the observed duration and magnitude are staggering, suggesting climatic conditions on the Earth that are perturbed to an extent not recognised elsewhere in the geological record and may have provided the impetus for the explosion of multicellular life.

Neoproterozoic negative $\delta^{13}C$ excursions appear entirely unlike negative $\delta^{13}C$ excursions observed in the Phanerozoic record in both magnitude and duration, and so the lack of a more modern analogue leaves the origin of Neoproterozoic excursions ambiguous. These isotopic excursions are commonly interpreted to record significant steady-state perturbations to the global carbon cycle, reflected in the carbon-isotope content of ocean waters. This oceanic signal is inferred to be preserved in Neoproterozoic carbonate successions due to several key criteria:

- Isotope values are reproducible spatially within basins and can be correlated with isotopic excursions of similar magnitude and duration in equivalent successions globally (Halverson *et al.* 2002, Halverson *et al.* 2005)

- Variation of this duration and magnitude appears to be restricted to the Neoproterozoic (Melezhik *et al.* 2005)

- Both negative and positive $\delta^{13}C$ variation is gradual and inferred to occur over millions to tens of millions of years (Fike *et al.* 2006, Le Guerroue *et al.* 2006, McFadden *et al.* 2008)

- Organic-rich pore fluids are unlikely to affect the carbon isotope composition of carbonates during diagenesis (Veizer *et al.* 1999)

Various writers have proposed mechanisms to account for a steady–state perturbation to the carbon cycle capable of skewing the C^{12}:C^{13} ratio to the scale recorded in Neoproterozoic carbonates (Hoffman *et al.* 1998, Fike *et al.* 2006, Bjerrum & Canfield 2011).

Recent contributions, however, have challenged the notion that the Neoproterozoic ^{13}C record preserves anomalous oceanic isotope values (Knauth & Kennedy 2009, Derry 2010, Swart & Kennedy 2011). Large magnitude negative $\delta^{13}C$ excursions recognised in the Neoproterozoic are widely interpreted to record variation of a primary oceanic origin. However, isotopic stratigraphic patterns of similar scale are observed in the Phanerozoic and are well documented, but are regarded as localised signals due to their disparity with the pelagic record and interpreted diagenetic origin. These Phanerozoic excursions are therefore not representative of the past isotopic composition of the Phanerozoic ocean (Swart & Kennedy 2011). Knauth & Kennedy (2009) present a model of overprinting by organic-rich meteoric fluids to account for significant negative $\delta^{13}C$ excursions in the Neoproterozoic, analogous to these well-documented Phanerozoic examples. This infers a diagenetic origin for the negative $\delta^{13}C$ anomalies in the Neoproterozoic, and would imply that these anomalies do not record major perturbations of the carbon cycle and are the result of overprinting of the carbon-isotope ratio by meteoric processes (Swart 2008).

Strongly negative $\delta^{13}C$ values (up to -9‰ in the Trezona Formation, South Australia (McKirdy *et al.* 2001) and -8‰ in the Ombaatjie Formation, Namibia (Halverson *et al.* 2002)) recorded in carbonate successions underlying Marinoan glacial deposits comprise the 'Trezona Excursion'. The isotopic excursion represents a sharp decrease in $\delta^{13}C$ from heavy values (~+8‰) to values on the order of -8‰ in carbonates stratigraphically below Marinoan glacial deposits. Similar magnitude excursions have been recognised in carbonate-dominated successions globally, including northern Namibia, north-west Canada, South Australia, Scotland, Norway and North America (Halverson *et al.* 2005). These sections are correlated with the Trezona Excursion by comparing patterns of isotopic change preserved in the stratigraphy; outliers are inferred to be incomplete fragments of section by proponents of a preserved primary $\delta^{13}C$ signal (Halverson *et al.* 2002). Significantly, independent timing constraints are not available to confirm this correlation.

The Trezona Formation of the Umberatana Group in the South Australian Flinders Ranges represents a classic succession dominated by carbonate rocks that records the Trezona Excursion: the pre-Marinoan glacial, negative $\delta^{13}C$ anomaly evident in the Neoproterozoic carbon isotope record of Halverson et al. (2005). The Trezona Formation preserves $\delta^{13}C$ values of as low as -9.5‰, which increases towards lighter isotopic values, up to -3‰. Despite being the namesake of the pre-Marinoan $\delta^{13}C$ anomaly, little work has been done to properly characterise the isotopes and lithologies stratigraphically, which becomes particularly relevant when considering the succession with regards to its diagenetic history. Previous workers have suggested that the Trezona Formation has undergone pervasive alteration and isotopic homogenisation, questioning the validity of chemostratigraphic data (Christie-Blick *et al.* 1999) and investigation of this would require higher resolution

stratigraphic data than has previously been reported. McKirdy et al. (2001) differs in the interpretation of a pervasively altered Trezona Formation interval on the basis that isotopic depletion observed in the Trezona Formation is no more severe than that observed in the underlying Etina Formation (McKirdy *et al.* 2001), which is accepted as unaltered (Christie-Blick *et al.* 1999). Furthermore, diagenetic cements are reported to be restricted to ooid and intraclastic limestones that return isotope values which are either verified by contiguous stromatolitic limestones or omitted from chemostratigraphic profiles (Burgess 1999, McKirdy *et al.* 2001). These observations appear consistent with data obtained by Singh (1986) in the Central Flinders Ranges, and therefore, the hypothesis of a formation-wide mechanism able to consistently perturb isotope values is discounted (Burgess 1999, McKirdy *et al.* 2001). More recently, Swanson-Hysell et al. (2010) suggest that the Trezona Formation may not actually preserve the isotopic variation associated with the Trezona Excursion in interpreted equivalent sections globally due to disparity in patterns of variation, specifically the Trezona Formation that approaches more positive values before the base of the Marinoan glaciation. This may suggest a more local origin of the isotopic variation observed in the Trezona Formation, contrary to oceanic isotopic signal hypotheses.

If the observed isotopic excursions are primary, and hence, the result of a significantly perturbed Neoproterozoic carbon cycle, the evolutionary implications are potentially staggering. It is reasonable to assume that a highly perturbed carbon cycle would likely apply significant evolutionary stress on early life, as is suggested by models describing the cessation of organic productivity leading up to glacial intervals (Hoffman *et al.* 1998). Conversely, a highly perturbed carbon cycle may have provided the impetus for the radiation of multicellular life during the Neoproterozoic. Significantly, Maloof et al. (2010)

reports clasts that appear to resemble simple sponge-grade metazoan fossils within intraclastic limestone units throughout the Trezona Formation. The occurrence of pre-Marinoan metazoan life questions current paradigms regarding the appearance of multicellular life and the conditions necessary for its radiation.

GEOLOGICAL SETTING

The Adelaide Fold-Thrust Belt in South Australia comprises upwards of 13km of dominantly shallow water Neoproterozoic sediments (Preiss 1987, McKirdy *et al.* 2001). The surface expression of the belt accounts for the Flinders Ranges and extends to the South through the Mount Lofty Ranges as far as Kangaroo Island. Current interpretation of the Adelaide Fold-Thrust Belt implies a passive continental margin undergoing several intracontinental sag-rift cycles, resulting in a deeply subsident Neoproterozoic to Cambrian basin complex (Preiss 2000).

The Umberatana Group in the Central Flinders Ranges comprises dominantly shallow-shelf and glaciogene successions, recording a history of transgressive-regressive cyclicity and glaciation (Preiss 1987, Preiss 2000) (Figure 1a, b). Accommodation space is broadly controlled by sag-phase subsidence (Preiss 2000), with local deposition in the Central Flinders Zone constrained topographically by diapiric activity and associated sub-basin formation (Lemon 1988). The upper Umberatana Group in the Central Flinders Ranges is defined by inundation and regional shelf-shale deposition, followed by what is interpreted to be a regressive cycle approaching the Marinoan glacial lowstand. Post-glacial flooding is marked by the laterally continuous 'cap carbonate' known as the Nuccaleena Formation (Preiss 1987).

Regional Stratigraphy

ENORAMA SHALE

The Enorama Shale is interpreted to record transgressive and regressive depositional environments in the lower and upper intervals of the unit respectively (Preiss 1987, Lemon 1988). The Enorama Shale varies in thickness to in excess of 400m, depending on paleotopography, interpreted to be a product of syn-depositional diapirism (Lemon 1988). The extensive distribution of the Enorama Shale and contiguous shale-dominated formations (Fig. 2) is indicative of broad inundation (Preiss 1996). Both the lower and upper intervals of the Enorama Shale comprise siltstones with minor carbonate lenses and hummocky cross-stratification and are interpreted as deepening and shallowing successions, respectively (Preiss 1987, Lemon 1988), with evidence of wave energy constraining water depths to above storm wave base. Dyson (1997) describes the Artipena Dolomite member of the Enorama Shale as the maximum flooding surface in the unit, with the Artipena Dolomite being sharply overlain by non-calcareous shale typical of the mid-Enorama and, according to Lemon (1988), indicative of stagnant, deeper shelfal deposition. Stromatolitic units fringing the western flank of the Enorama Diapir (Lemon 1988) allowed for chemostratigraphic analysis of the formation by McKirdy *et al.* (2001), returning relatively constant $\delta^{13}C$ values of +6‰ to +7‰. A U-Pb age of 657 ± 17 Ma on detrital zircons of the Marino Arkose member of the Enorama Shale is presented by Ireland et al. (1998).

TREZONA FORMATION

The Trezona Formation is interpreted to be the shallowing-up continuation of the regression interpreted in the upper Enorama Shale, approaching the glacial lowstand of the overlying Elatina Formation (Lemon 1988, McKirdy *et al.* 2001, Williams *et al.* 2008). The Trezona Formation reaches thicknesses of up to 400m and represents the last major carbonate

succession of the Umberatana Group prior to the Marinoan glaciation. Spatial distribution of the Trezona Formation is highly restricted, confined to the Central Flinders Zone (Fig. 2). The lower Trezona Formation comprises dominantly shales and rippled siltstones with carbonate concretions. Shales are interbedded with dominantly intraclastic breccias and minor sandstones, algal laminates and stromatolite mounds. Metre-scale grainstones form resistant bands of outcrop, are generally homogeneous and are interpreted as ooid shoal deposits (McKirdy *et al.* 2001). The upper Trezona Formation is dominated by stacked stromatolite mounds with minor ooid grainstone and intraclast beds.

The Trezona Formation is interpreted to have been deposited in a shallow shelf environment with a lagoonal and partly tidal component (Preiss 1987, Lemon 1988). Interbedded shales comprising the lower interval of the Trezona Formation are suggested to shallow-up through an ooid and intraclastic barrier-bank system protecting a shoreward lagoonal or tidal flat area dominated by stromatolite sequences (Lemon 1988). A partly tidal interpretation is based on evidence of shallow water deposition, periodic exposure and desiccation, preservation of cross-laminated sands, and elongate stromatolite morphologies (Preiss 1987).

YALTIPENA FORMATION

The Yaltipena member is up to 100m in thickness and comprises basal laminated, fine sandy, muddy siltstones grading into sands that coarsen up from fine- to medium-grained. Channelised, clean quartz sandstones preserving ladder and interference ripples occur contiguous with evidence of exposure in mudcracks, rare halite casts and possible raindrop impressions, suggestive of a very shallow, consistently exposed depositional environment. A disconformable surface at the base of the Yaltipena Formation has been identified proximal

to the type section, leading previous authors to suggest that the Yaltipena represents its own discrete depositional cycle and disconformably overlies the Trezona Formation. The Yaltipena member is more restricted in distribution than the Trezona Formation (Figure 1, 2), with erosion along sequence boundary at the base of the glacigenic Elatina Formation assumed by previous authors to have removed the Yaltipena from the northern and southern ends of the Trezona Range. Despite evidence of constant exposure and spatial restriction, previous interpretations of the Yaltipena Formation is of a transgressive-regressive depositional cycle, with the silty lower interval being deposited in slightly deeper water followed by a shallow subtidal to tidal flat environment (Lemon & Reid 1998).

ELATINA FORMATION

The Elatina Formation comprises ~60m of dominantly pinkish, massive, fine-medium, feldspathic sandstones derived from glacial outwash. Diamictic lenses include clasts sourced from underlying strata (McKirdy *et al.* 2001) and dropstone-bearing siltstones occur in what are inferred to be post-glacial, regionally deeper-water settings (Preiss 2000).

SAMPLE COLLECTION AND ANALYTICAL METHODS

Stratigraphic Logging

Exposure of the Trezona Formation in the Trezona Range and the Little Bunkers Range was the focus of stratigraphic logging, with measured sections being constructed at the two localities outlined in Figure 1a. Observations were also made at Bull's Gap and Enorama Creek in order to characterise the basal succession of the Trezona, which is covered in the Little Bunkers Range and Trezona Range sections. The locations logged were chosen based on completeness of exposure and spatial distribution in an attempt to characterise variation across the extent of the formation, and therefore, give evidence for variations in the

depositional and diagenetic history of the basin. Each section was logged using a 1.5m Jacob's Staff and Brunton Compass, following the technique outlined by Compton (1985). Lithofacies were described in the field and stratigraphy was grouped by lithology and logged accordingly at a bed scale.

Samples were collected across the four localities (Figure 1a) and were selected in the field based on lithological changes, rather than at regular intervals, in order to account for as much stratigraphic variation as practicable. Textural variation within lithofacies was also sampled for in order to characterise the extent of recrystallization within each lithology.

Petrographic Analysis

Thin sections of samples representative of each lithology were prepared and analysed under reflected light microscopy. Further samples were then analysed petrographically to account for variation within each lithology. The purpose of the petrographic study was primarily to observe the textural properties of the samples and to infer possible primary and diagenetic controls. Petrographic observations also guided microsampling for isotope analysis. Thin sections were stained using the staining techniques outlined by Dickson (1965) to differentiate between calcite, Fe calcite, dolomite and Fe dolomite in key samples.

Carbon and Oxygen Isotope Analysis

The δ^{13}C and δ^{18}O values of samples from the three sections were obtained using Isotope Ratio Mass Spectrometry. The Blinman section was used as a chemostratigraphic reference section, with 110 samples being analysed for δ^{13}C and δ^{18}O over ~235 m of stratigraphy. Following petrographic analysis, subsamples of specific components were microdrilled and analysed for δ^{13}C and δ^{18}O to determine heterogeneity of the values between different textural components of the samples and to supplement diagenetic interpretations.

Powdered samples were collected by microdrilling fresh rock surfaces and slabbed samples to produce a fine powder. Different textural components of each sample prepared were microdrilled separately. δ^{13}C and δ^{18}O were measured simultaneously at the University of Adelaide on a Fisons Optima isotope ratio mass spectrometer (IRMS) with dual inlet IRMS coupled to a Fisons Isocarb carbonate preparation system. Measured data were calibrated against an in-house calcite standard (ANU-P3; δ^{13}C (VPDB) = 2.24‰; δ^{18}O (VPDB) = -0.30‰). Total analytical errors (1s) for δ^{13}C and δ^{18}O are estimated at ±0.07 and ±0.15‰ based on repeat analyses of standards.

RESULTS

Sedimentology

LITHOLOGICAL UNITS

Shale: Non-Calcareous, grey-green to red-brown, fissile mudstones. Beds are 1-3 cm in thickness with distinct resistant beds of 2-5 cm thick siltstone. Resistant beds are well laminated and often preserve ~15 cm ripple cross-laminations (Figure 3a). Elongate-rounded calcareous concretions (5-15 cm) are abundant throughout the shale facies and represent the only carbonate component of the shale facies. Shale beds are interbedded with flakestone breccia facies beds, which have sharp bases.

Flakestone Breccia: Flake-clasts of microbial laminites, stromatolites and/or laminated marl supported by a micritic-microspar matrix. Clasts are elongate, flat, dominantly micritic flakes, generally ranging between 5-20 mm long and 1-5 mm in thickness. Clasts are usually aligned parallel to each other and are loosely continuous to bedding, although locally clasts often 'stack' perpendicular to bedding or form radial rosettes, suggesting high energy deposition (Figure 3b). Flakestone breccia beds have undergone varying degrees of

recrystallisation of both matrix and clast material. Crushed clast textures are common, with the interiors of crushed clasts usually replaced with microspar, which is continuous with matrix mosaics. Beds are commonly dissected by styolites that truncate matrix material and clasts. The flakestone breccia facies commonly occurs as discrete, sharp based, resistant horizons, dominantly interbedded with the shale facies and often oscillate in thickness along strike. Beds are not laterally continuous and are typically 5-20 cm thick. Commonly, flakestone breccia beds fine up into a 1-5 cm marl interval with or without mudcracks (Fig. 3c). Occasional stromatolite and carbonate-cemented fine-sand beds overlie flakestone breccia beds. This facies is likely to represent storm event deposition, with intraclasts being transported from a proximal, desiccated stromatolite or laminated marl source, with overlying marl beds marking the transition back to a lower energy depositional environment.

Intraclastic Grainstone: Clasts derived from other lithologies within the formation (oolites, laminated marl, micritic flakes) supported by a micritic matrix, often recrystallised to coarse spar. Clast sizes are highly variable, ranging from 0.5-3 cm in width and are flat, 1-5 mm thick flake-clasts or subrounded-rounded, equant oolite or laminated marl clasts. Some intervals are sharply interbedded with centimetre-scale marl layers. Heavily dissected with styolites and centimetre thick dissolution seams, which resist weathering relative to the matrix (Fig. 3d). Surficial layering shows a stacking pattern of decimetre layers with intervening reactivation surfaces. Intraclastic grainstones occur as several metres thick, resistant intervals in the mid-upper Trezona Formation. Commonly interbedded with 1-5 cm marl layers. Likely representative of cyclic debris flow, probably storm driven, within a local depocentre.

Oolite: Dominantly ooids supported by a micritic-microspar matrix. The majority of ooids observed are sub millimetric (commonly 0.2-1 mm) and occur in varying abundances relative to matrix material within each oolitic interval. Ooids are either micritic with remnant textures preserved by insoluble materials, or are replaced by dominantly microspar-pseudospar with little ooid texture. Styolites and dissolution seams dissect the unit with dissolution seams often concentrating pelitic sediment. Oolites dominantly occur as metre-scale resistant beds in the mid-upper Trezona Formation and are often interbedded with 1-5 cm marl layers and lenses. Upper interfaces between oolites and overlying strata are generally sharp based. Oolites tend to occur interbedded with decimetre stromatolite and algal laminate beds with stromatolite mounds occasionally growing directly above ooid units.

Stromatolites: Decimetre-metre thick stromatolite mounds. Mounds have 1-3 cm layering defined by silty horizons with trapped, subangular quartz grains. Pelitic layers are more resistant to weathering than the matrix material. Stromatolites occur as either well-formed, cumulate domes (Figure 3e), with bases conforming to the surface of underlying beds or poorly formed 'loaf' shaped structures likely to have grown depending on local current action. Associated primarily with the upper Trezona Formation interval and often overly oolite, redbed sandstone and intraclastic grainstone facies (Figure 3f). Likely to have formed in a relatively deep-water environment due to the lack of preserved desiccation surfaces seen in the lower Trezona Formation.

Microbial laminites: Well laminated, flat, layered microbial mats (Figure 3g). Dominantly micritic with internal layering defined by resistant, 1-5 mm spaced, millimetric horizons of

silt and very fine, subrounded quartz grains. Commonly occur as ~ 1m beds overlying oolite beds or as decimetre scale successions of stacked microbial mats.

Carbonate-Cemented Fine Sand: Well sorted, angular-subangular, equant fine sand with a micritic carbonate cement. Sand is micaceous with 0.5-1 mm, bladed muscovite flakes orientated according to the internal layering. Typically comprises 5-10% carbonate, 5% muscovite and 85-90% quartz, however some examples fine up into fine sandy marl layers (1-3 cm in width). Laminations are defined by layers of variable abundances of cement relative to quartz. Some exposure preserves cross-laminations. Carbonate cemented fine sands occur as resistant beds interbedded with the shale facies in the lower Trezona Formation interval.

Redbed Sandstone: Interbedding of dominantly well laminated red siltstone and micaceous fine sand diagnostic of the Yaltipena Formation. Sand beds are decimetre-bedded with coarse laminations, while silt interlayers are 5-30 cm thick and locally fissile. Beds are occasionally gritty. Redbed sandstones occur primarily at the upper contact as part of the Yaltipena Formation overlying the Trezona Formation. Distinct lensoidal bodies, ~5m wide with sharp bases (likely channels) occur within the Trezona Formation and are often overlain by stromatolite units.

Marl: Massive to laminated micrite occurring as centimetre-thick beds (Figure 3h). 0.5-2 mm laminations defined by darker horizons.

TREZONA RANGE SECTION

The Trezona Range measured section (Figure 4) encompasses ~350m of stratigraphy, with the lower succession being exposed directly off of the road to Blinman, approximately 19km south of the town. The basal contact of the section is covered, however; for reference,

proximal basal sections at Bulls Gap and Enorama Creek are documented in subsequent sections of this manuscript. The lowest exposure of the Trezona Formation in the Trezona Range comprises primarily interbedded shale and intraclastic algal-flake breccia facies. Typically 5-30 cm thick flakestone breccia beds, which oscillate in width laterally, sharply interbed with 5-15m units of centimetre-bedded grey-green shale, preserving internal cross beds and rippled laminations in sporadic resistant beds. Resistant beds are typically 1-5 cm in width and are non-fissile. The lower-Trezona shale facies also preserves ~ 10 centimetres, elongate carbonate concretions. The first carbonate-cemented fine sand and stromatolite beds occur at a stratigraphic height of ~53 m. Stromatolite beds occur directly above carbonate-cemented fine sand and flakestone breccia facies and are sharp based. The first major resistant band in the section comprises a reddish, 1m carbonate-cemented fine sand bounded by 2 ~1 m thick sequences of massive intraclastic grainstone, preserving algal flakes and marl rip-up clasts and lenses orientated continuous with the bedding plane. A stratigraphic height of 78-87 m marks the return to interbedded shale and algal-flake breccia facies with a decrease in the concretionary component of the shale facies. Overlying this is the first of several massive, oolite bars which occur laterally persistent across several kms of exposure along strike.

Overlying strata continues the trend of interbedded shale and flakestone breccia facies with increasingly abundant carbonate-cemented fine sand and stromatolite beds associated with the flakestone breccia facies. Stromatolites tend to overlie erosional surfaces on flakestone breccia beds and are transitional with red carbonate-cemented fine sands. The next major resistant unit occurs at a stratigraphic height of 138-155 m. The unit is comprised of a dominantly microspar-matrix intraclastic grainstone and is highly dissected by styolites.

Centimetre-thick dissolution seams throughout the unit result in a surficial cross-cutting layering. Petrographic analysis reveals that a concentration of blocky-spar, rounded, elongate clasts (reminiscent of those observed in lower Trezona flakestone breccia beds) are preserved within dissolution seams.

At a stratigraphic height of 210-265m microbial laminate beds become common, often overlain with decimetre-thick intraclastic breccia beds. Microbial laminates appear restricted to this interval for the most part, which coincides with the occurrence of more numerous ooid grainstone beds. Sections of this interval are covered and so the underlying lithology remains enigmatic, however, due to the nature of lithological cyclicity earlier in the section and the resistance of interbeds to weathering, we could speculate that covered section is likely shale dominated. Oolite and intraclastic grainstone beds within the 220-310m interval often preserve micritic envelopes nucleated around clasts. Crushed clast fabrics and blocky calcite matrix cements are also prominent in this interval.

The uppermost 50m the Trezona Range section preserves stromatolite, oolite, and intraclastic grainstone beds up to several metres in thickness. Field observations show that stromatolite mounds appear to contour to the upper surface of oolite and intraclastic grainstone facies. The highest exposure and corresponding dip-slope comprises stromatolite mound facies. ~1.5 km to the South, the Trezona-Yaltipena interface is exposed in a creek cutting. The uppermost surface of the Trezona Formation is dominated by a palaeokarst surface, infilled by a collapse breccia of marl blebs supported by a micritic matrix. Matrix material also supports crushed microbial-flake intraclasts. Marl blebs range from granule-cobble size, with rounded margins. Overlying the karsted interval sharply is a sequence of massive to centimetre bedded marl, which coarsens into the red, interbedded, micaceous

fine sands and shales of the Yaltipena Member. Significantly, the Yaltipena has been observed interbedding the upper stromatolite interval of the Little Bunkers Range and Blinman sections, suggesting that the karst surface is likely a regional feature, possibly related to local diapiric influences, and does not represent a sequence boundary.

LITTLE BUNKERS RANGE SECTION

The Trezona Formation outcrops for over 400m in the Little Bunkers Range through 2 major topographic rises (Figure 5). Again, the basal contact with the Enorama Shale in the Little Bunkers Range is covered. Due to extensive cover, the measured section begins approximately 75 m stratigraphically above the inferred position of the basal contact. The lower section is dominated by concretionary shale facies, interbedded with resistant bands of reddish, well laminated carbonate-cemented fine sands and flakestone breccias with 1-3 cm marl interlayers, both sharp based. Carbonate-cemented fine sands and resistant shale beds often preserve internal cross-beds and marl layers, with several resistant shale beds preserving mud cracks.

A stratigraphic height of 5-35m preserves cycles of flakestone breccias, oolite beds and cumulate stromatolite domes. Stromatolites generally occur sharply overlying successions of interbedded flakestone breccias. The subsequent ~35m transitions back into dominantly interbedded shale and flakestone breccia facies, with sharp based, carbonate-cemented, laminated fine sands and sharp based stromatolite and algal laminite beds. This interval preserves mud cracks in many of the marl 'caps' typical of the flakestone breccia facies. This preservation of mud cracks in marl beds associated with flakestone breccia beds continues between stratigraphic height ~100-180m. At a stratigraphic height of ~137m, centimetre-decimetres interbeds of marl, intraclastic grainstone facies and covered beds comprise ~6m

of stratigraphy. Approximately 20 couplets of intraclastic and marl facies are identified, with intraclastic beds ranging from 3-25 cm in width and marl beds from 1-6 cm in width. All beds are sharp based, with the lower intraclastic grainstone beds containing ooids and the upper intraclastic beds preserving highly recrystallised, crushed, elongate clasts and lacking ooids. The upper marl layers preserve mudcracks. A stratigraphic height of approximately 155m marks a transition to shale and laminated carbonate-cemented fine sand facies, with loaf-shaped stromatolite mounds typical of the lower Trezona interval in the Little Bunkers Range and mud cracks preserved in flakestone breccia marl layers.

The Little Bunkers Range comprises a number of gentle topographic inclines and declines, the steepest of which comprises the stratigraphic interval of approximately 100- 220 m. The topographic high of the range comprises a steep, highly resistant band of up to 50 m of dominantly oolite facies. The base of this succession comprises a decimetre thick, laminated, carbonate-cemented sand bed, overlain by a sharp-based, highly irregular microbial laminite which conforms to the surface of the underlying bed. This is overlain by a flat algal mat, which is in turn overlain by a ~1m bed of oolite. The subsequent 5-6 m of section comprises a regularly interbedded marl and sandy marl unit, with 5-15mm interbeds of less resistant marl and 3-8 mm interbeds of resistant sandy marl. Layering of the interbeds is undulating, with lenses of marl defined by more pelitic margins being common.

The topographic high of the Little Bunkers Range and the subsequent dip-slope is comprised of a massive, broadly homogeneous oolite. Surficial layering observed in the field is the product of dissolution seams, which through petrographic analysis are observed throughout much of the sequence. This mid-Trezona interval is dominantly comprised of recrystallised oolites, often replaced with blocky spar, supported in a fine-spar matrix with minor angular

quartz and silt grains. Dissolution seams are seen to be truncated by veins, suggesting early-stage pressure solution alteration. The subsequent dip-slope comprises the first of two major packages of stromatolite mounds.

An oolite interval at ~245m is overlain by a ~7m thick succession of intraclastic grainstone. Significantly, this unit preserves clasts described by Maloof et al. (2010) as relict, sponge-grade body fossils (Figure 6a). The unit occurs as a metres-bedded bar with 2-3cm layers of matrix-supported clasts. Layering is defined by 5-10mm thick sandy horizons. Intraclasts comprise curled flake-clasts, 0.5-2cm wide with extensive recrystallisation evident in hand specimen (Figure 6b). Petrographic analysis reveals that intraclasts are entirely replaced by mosaics of 0.2-1mm pseudospar crystals and are supported by a micritic matrix (Figure 6c, d).

 The uppermost interval of the Little Bunkers Range section comprises a ~65m thick succession of stromatolite mounds. At 325 m, a single bed of 70 cm thick redbed sandstone interbedded with stromatolites. The top contact of the Little Bunkers Range section coincides with a mudcracked algal laminite stratigraphically below non-calcareous, well bedded, reddish fine sands with minor carbonate cements.

BULL'S GAP BASAL CONTACT

The basal contact between the Trezona Formation and the underlying Enorama Shale is exposed in a creek bed adjacent to the Flinders Ranges National Park boundary at Bulls Gap. The Enorama Shale is identified by a sequence of non-calcareous, grey-green laminated siltstones analogous to those observed at the base of the Trezona Range section. Laminations are laterally uniform and no ripples or storm beds are identified until ~3 m stratigraphically below the contact. Storm beds consist of sharp based, ripple laminated

fine-medium grained sandstones. The contact itself is interpreted to be the lower surface of a ~10 cm rippled fine sand- siltstone bed with silty drapes. Mud cracks are preserved in this interval, suggestive of a period of exposure.

Immediately overlying the mudcracked exposure surface is a ~20cm interval of subangular blocky aggregates, reminiscent of soil peds but lithified, supporting tabular, dominantly mud and siltstone, fragments. This layer penetrates up to 5 cm into the underlying bed through spaces between clasts. While this interval does not preserve any evidence of stratification or sorting, it does occur parallel to the underlying Enorama Shale. Transitional clast margins and preserved rippled bedding within fragments at the base of the interval indicates in-situ weathering of Enorama Shale. This aggregated interval is therefore interpreted as a paleosol, characterising an unconformable surface at the base of the Trezona Formation. The upper surface of this layer is an interval of ~1 m thick Trezona Formation shales, analogous to those observed at the base of the Trezona Range section, which contour to the upper surface of the palaeosol. A ~10 cm horizon of carbonate cemented siltstone interbedding the non-calcareous shale represents the first carbonate bed preserved here. The upper limit of this exposure is defined by a ~20 cm thick, sharp based, intraclastic algal-flake breccia bed which is highly recrystallised. ~50m along strike, further exposure suggests a transition to interbedded concreted shales (calcareous) and intraclastic algal-flake breccias, analogous to the lower Trezona Formation succession observed in the Flinders Ranges section (Figure 4).

ENORAMA CREEK BASAL CONTACT

The basal contact between the Trezona Formation and upper Enorama Shale is exposed in Enorama Creek. Exposure extends for ~100 m to the east and north in a low cliff, suggesting

that the contact is a laterally continuous feature. The contact is abrupt, with 80 cm thick cumulate stromatolite domes orientated parallel to each other sharply overlying centimetre bedded, non-calcareous shales, continuous for tens of metres below the contact (Figure 7). Stromatolites do not occur below the contact, nor do similar shales overlie the contact suggesting an abrupt shift in sedimentation following a period of erosion. Stromatolites are overlain by 2 m of non-calcareous, 1-3 cm bedded shales followed by a ~ 1 m intraclastic grainstone bed, an association that is readily observed in the lower Trezona formation several kilometres south along strike. Similarly, the underlying shale succession is devoid of carbonate in the vicinity of the contact and is similar to Enorama Shale recognised at the base of the Trezona Range section.

Carbon-Oxygen Stable Isotope Patterns

Stable isotopic values were analysed in 3 measured sections (Trezona Range, Little Bunkers Range, Blinman region) and compared to data from Maloof et al. in the Bunkers Range near Emu Gap (Figure 1). A higher resolution interval (M Kennedy pers. comm.), also from the Little Bunkers Range, was analysed. Samples were collected primarily to investigate isotope variability in association with lithological change, though were collected in measured sections and can hence be considered in conjunction with previous chemostratigraphic studies (McKirdy *et al.* 2001, Maloof *et al.* 2010). These data show similar depleted values in the lower Trezona Formation (>-9‰ δ^{13}C and -14‰ δ^{18}O) which are reported to shift towards heavier δ^{13}C values of -2‰ in the upper interval.

Patterns between the primary reference sections at Bulls Gap (Figure 7) and Blinman (Figure 8) show substantial differences in magnitude and shape of δ^{13}C and δ^{18}O when compared against stratigraphic height. While both isotopic profiles record a distinct shift toward

heavier δ^{13}C values in the upper interval, this occurs over 160m in the Emu Gap section and only 20 m in the Blinman section. In both cases, this transition occurs in association with the lithological shift to stromatolitic textures and a pronounced inflection point in δ^{13}C is noted at the base of the stromatolite facies. A +6‰ progressive shift is observed confined to upper stromatolite facies in both sections. The disparity in thickness of stromatolites hosting the δ^{13}C isotopic shift could be associated with a facies change or could alternatively be due to localised erosional truncation.

While δ^{13}C values are consistently on the order of -8.5‰ throughout the majority of the Blinman section and the lower ~130m of the Emu Gap section, some notable deviations are evident. δ^{13}C values at 125m and 133m in the lower Blinman section are anomalously heavy relative to the general isotopic trend, reaching values of -4‰ and -5.4‰ respectively. This variation occurs within carbonate-cemented fine sand facies and adjacent concreted beds. In the Emu Gap section, a ~1.0‰ step in δ^{13}C to heavier values is observed at ~130m which is restricted to an interval of interbedded grainstone, stromatolite and microbial laminate facies. Detailed study of the 170-230m interval shows a second order, cyclic pattern of increasingly positive δ^{13}C values. This variation occurs as a component of the overall trend to heavier δ^{13}C values and may indicate environmental cyclicity in a more discrete system. A regression of δ^{13}C in the upper Emu Gap section (265m) of ~1‰ is observed and is not reflected in the Blinman section, possibly due to truncation of the upper Trezona Formation in the Blinman section.

δ^{18}O values recorded in the Blinman section are dissimilar to those at Emu Gap, other than in their initial magnitude of -14‰. These highly depleted values are retained throughout in the Blinman section except at 125m, where values in carbonate-cemented fine sands rise to

-3.7‰. A strong stratigraphic trend is evident in the Bulls Gap section where $\delta^{18}O$ values show systematic change with stratigraphic height. An initial progressive shift to more positive $\delta^{18}O$ values is observed until ~160m, where $\delta^{18}O$ values become stable. Detailed study of the interval between 180m and 220 m (Figure 11) suggests that a second order pattern in $\delta^{18}O$ variability of 2‰ is superimposed on the broader trend. The cause of this is not evident but could be associated with non-marine primary fluids (given the depleted ^{18}O) or systematic mixing associated with lithological change. Significantly, the ~1‰ increase in $\delta^{18}O$ observed at 205m occurs with the first appearance of oolite facies, supporting a lithological association with more positive values. In general, $\delta^{18}O$ values throughout both sections are strongly depleted, reflecting meteoric or thermal influence with no indications of a marine signal. Comparison with $\delta^{18}O$ data from the Etina Formation from Maloof et al. (2010) shows a similar range of $\delta^{18}O$ from -3 to -12‰ as in section 8. The heavier values argue against a thermal resetting.

When cross plotted, $\delta^{13}C$ and $\delta^{18}O$ values from the Emu Gap section displays three distinct isotopic trends corresponding with lithological associations in the lower shale, middle grainstone and upper stromatolitic stratigraphic intervals (Figure 9). Isotope values show both covariant and divergent relationships within shale and stromatolitic intervals respectively. In the lower interbedded shale facies from the base of the section to a stratigraphic height of ~ 130m, $\delta^{13}C$ and $\delta^{18}O$ values show a positive covariation with a regression of 0.9 (Figure 9). Much of this carbonate is evident as cements within concretions, and it comprises the most $\delta^{13}C$ depleted values (< -6‰ to -9‰) defining the "Trezona Anomaly" commonly correlated globally. A ~1.0‰ shift in $\delta^{13}C$ to more positive values at 130-150m coincides with $\delta^{18}O$ values that are highly varied, ranging from -11.4‰

to -7.6‰. This interval is closely associated with a sequence of interbedded stromatolites, microbial laminites and grainstones, and may reflect local mixing of meteorically-derived pore fluids within grainstone facies. Diverging δ^{13}C and δ^{18}O patterns in the upper stromatolitic interval produce a broadly negatively correlated relationship. Divergent isotopic systematic are not considered indicative of an oceanic signal due to the discrete controls on δ^{13}C and δ^{18}O variation in an open marine setting. This signal may represent increasing meteoric input in a system becoming progressively more open, while organic productivity shifts δ^{13}C above mantle levels not recorded in the lower Trezona Formation (Melezhik *et al.* 2005).

Discrete, systematic trends are observed in the Emu Gap section where δ^{13}C and δ^{18}O values are cross-plotted (Figure 9). Trend A) is associated with a 2m thick microbial laminate interval of the lower shale facies at a stratigraphic height of 15m and shows a positive covariance of δ^{13}C and δ^{18}O values. If values are considered primary, depleted δ^{18}O values are indicative of meteoric input implying a non-marine control on isotope variation. Conversely, trend B) illustrates a negative correlation between δ^{13}C and δ^{18}O values and is also associated with a microbial laminate interval, occurring at a stratigraphic height of 201m.

The apparent covariance observed in the lower Emu Gap and Blinman, shale-dominated intervals is supported by a subset of values derived from the lower interval of the Little Bunkers Range section (Figure 10a). Samples taken over 9m of section show a cyclic variation in both δ^{13}C and δ^{18}O values of 7.6‰ and 5.4‰ respectively. These samples represent an interval of concretionary shale facies, interbedded with resistant beds. Depletion of both δ^{13}C and δ^{18}O to <-8‰ and <-10‰ occurs in conjunction with resistant

beds, suggesting that the abundance of concretionary carbonate is a first order control on isotopic variation in this interval. Less-depleted values (-3.4 to -7.9‰ δ^{13}C and -6.4 to -9.6‰ δ^{18}O) are associated with marl and less concreted intervals. Of note is the strong covariance observed in this interval; variation of up to 7.7‰ δ^{13}C is mirrored by associated δ^{18}O values. The cyclic variation in δ^{13}C and δ^{18}O is indicative of a mixing relationship, with the most isotopically depleted values being the most heavily concreted shale intervals. Due to the inferred early depositional origin of carbonate concretions, isotopic depletion may be associated with mixing of early burial fluids. Variation of this magnitude over such a small interval is problematic for a primary marine origin.

Diagenetic Textures

Field observations of shale concretions typical of the lower Trezona Formation (Figure 4) suggest early-stage carbonate precipitation within unconsolidated sediment. Concretions occur as 5-15cm lenses of carbonate-cemented siltstone which pinch out into contiguous shale beds. The lack of concentric structure indicates a pervasive mode of concretion (Raiswell & Fisher 2000). Concretions occur restricted to the lower Trezona shale facies, which occurs coincident with steady-state depletion of δ^{13}C and δ^{18}O values, suggesting a potential control on isotopic depletion related to concretions or from mixing of pore fluids derived from dissolved concretionary phases.

Petrographic investigation of a lower Trezona Formation flakestone breccia at 11m (sample 26.4.11.7) illustrates the development of early microspar cements filling interparticle porosity. Clast interiors are dominantly micritic, with selective dissolution of some clasts resulting in replacement by coarse pseudospar which appears continuous with interparticle spar mosaics, suggesting that intraparticle recrystallisation occurred synchronously with

precipitation of pore-filling cements (Figure 14a). Later-stage styolites (Figure 14b) readily truncate micritic intraclasts and matrix spar, reinforcing an early-burial origin of pore-filling cement precipitation. This sample occurs in the same interval associated with carbonate concretions in shale facies, and highly depleted δ^{13}C and δ^{18}O values (<-10‰ and <-11‰ respectively) are present. Microsampling of individual components returns relatively homogeneous values, with variation of up to 1.5‰ in δ^{13}C values of clasts and matrix material.

Micritic envelopes are preserved in flakestone breccia, intraclastic grainstone and oolite facies, sporadically within both the Trezona and Little Bunkers Range sections. Sample 27.4.11.83 preserves micritic envelopes around the majority of clasts in an intraclastic grainstone from the upper Trezona Range section. Relic micritic rims (Figure 13c) suggest that precipitation of interstitial cements succeeded the dissolution of clast interiors, due to matrix mosaics being continuous with intraparticle cements.

Sample 27.4.11.44 (Figure 13d) indicates compositional variation spatially within interparticle cements. Fe calcite spar is localised around intraclasts in the form of isopachous fringing cements. Pore space is filled by a microspar precipitate that is lacking in Fe. This is suggestive of multiple stages of precipitation of pore-filling cements facilitated by pore fluids of different elemental compositions.

Figure 13e shows extensive recrystallisation of oolite sample 30.4.11.55 from the middle Little Bunkers Range section. A single microspar phase dominates the sample, with matrix and intraparticle spar occur continuous with each other, suggesting complete recrystallisation of primary calcite and early burial cements. Conversely, Figure 13f illustrates varying degrees of recrystallisation within sample 30.4.11.92 (Little Bunkers

Range, 256m), preserving: a) micritic ooids with little internal texture, b) dominantly micritic ooids (with concentric textures) with the inferred formation of intraparticle porosity and subsequent precipitation of microspar within pore space and c) concentric micritic ooids with selective dissolution of intraparticle calcite and subsequent replacement with single coarse-spar crystals.

DISCUSSION

Depositional Environment

Current interpretations of the Trezona Formation depositional environment are inconsistent with observations presented in this study. Previous authors have described the Trezona Formation as deposited in a marginal marine environment, likely lagoonal and partly tidal in nature (Preiss 1987). A tidal interpretation is based on evidence of shallow water deposition, periodic exposure and desiccation, preservation of cross-laminated sands, and elongate morphologies of stromatolite mounds (Preiss 1987). However, no evidence of unique features of tidal environments such as current reversal or tidal bundling has been reported, and the sedimentary features reported are common to a variety of shallow water depositional environments. Lemon (1988) presents a model of a simple homoclinal ramp with lime mud deposition dominating the shoreline and stromatolites occurring in a shoreward lagoon or tidal flat position. This interpretation suggests that the stromatolite facies transition is indicative of shallowing conditions, implying that the Trezona Formation is regressive in nature. Several observations presented by this study, however, cast doubt on these interpretations.

The stratigraphic context of the Trezona Formation following shelf shale deposition in the Enorama Shale has commonly led to the conclusion that the Trezona represents simple first

order shallowing-upward toward the glacial lowstand of the Elatina Formation. This implies a conformable transition towards shallow-water carbonate deposition as a continuation of the overall regression expressed from the upper Enorama Shale to exposure and erosion at the top of the Trezona Formation. The study of the contact between the Trezona Formation and the Enorama Shale and the Trezona with the overlying Elatina and Yaltipena Formations suggests a more complicated relation to water depth. A conformable contact with the underlying shelf muds of the Enorama Shale is often assumed for the lower Trezona Formation, which is rarely exposed. However, exposure of the contact at Bulls Gap and in Trezona Creek preserves a sharp discontinuity between the Enorama Shale and Trezona Formation in both cases. The Trezona Formation observed at Bulls Gap indicates that deposition of the lower Trezona Formation followed exposure of the Enorama Shale for a period long enough for a soil horizon to develop. Similarly, the contact observed in Trezona Creek preserves an abrupt step to stromatolitic limestone from shelfal muds of the Enorama Shale across a single bed. The apparent sharp interface and apparently regionally traceable surface between the lower Trezona Formation and upper Enorama Shale is suggestive of a break in sedimentation, followed by a flooding event, which qualifies as a sequence boundary in the nomenclature of Van Wagoner et al., (1990).

Observed in the lower portion of the Little Bunkers Range section is an interval ~ 150 m in thickness preserving mudcracks, primarily in the micritic 'caps' overlying flakestone breccia storm beds, which is consistent with frequent variation of water depth, including exposure, and not of a single shallowing trend. Mudcracks occur confined to interbedded shale and flakestone facies, suggestive of a sustained history of repetitive exposure. Shelf models proposed by Lemon (1988) are less consistent with periodic exposure, with limited evidence

of a return to deeper water conditions. In previous interpretations (Lemon 1988) interbedded shale and flakestone facies are assumed to be deeper water successions with respect to stromatolite facies, which are restricted to shallow tidal flat and lagoonal areas in these models. The presence of mudcracks in these mud dominated facies, and the lack of features indicating desiccation in the stromatolite facies comprising the upper Little Bunkers Range section is indicative of an environment that broadly deepens up-sequence, again contrary to interpretations of the Trezona Formation as regressive.

The Yaltipena Formation is identified in the upper part of the Little Bunkers Range and Trezona Range measured sections, but is absent in the Blinman and Emu Gap sections. The Yaltipena has been reported to unconformably overly the Trezona Formation in the Central Flinders Ranges (Lemon and Reid, 1988) implying a sequence boundary preceding the Elatina Formation. However, channelized beds of 0.5-1 metres comprised of red-bedded, micaceous fine sands identical to those comprising the Yaltipena Formation are interbedded with stromatolitic intervals characteristic of the upper Trezona Formation in the Little Bunkers Range and Blinman sections, suggesting that the Yaltipena Member represents a fluvial facies change that interfingers with stromatoltic environments. Interbedding argues strongly against a significant break or unconformity separating the Trezona and the Yaltipena. It does imply that fluvial and subaqueous stromatolitic environments may have been contemporaneous. Deposition of the Yaltipena Formation may be synchronous with the Trezona Formation in part. Despite the Yaltipena Formation being missing in this section, the Blinman section presented in this study also preserves discrete beds of red-bedded, micaceous fine sands in its uppermost interval.

The culmination of these observations suggests that a model of simple first order shallowing up from the shelfal muds of the Enorama Shale to the shallow-water carbonates of the Trezona Formation is inadequate. The Trezona Formation represents its own depositional cycle, distinct from the Enorama Shale, which appears to broadly deepen rather than shallow-upwards and is shallow for tens to hundreds of metres of section. This implies a significant time break following the deposition of the Enorama Shale and questions the assumption that the Trezona Formation represents the continuation of the regression observed in the upper Enorama, due to the limited evidence supporting a lagoonal and tidal origin for the Trezona and the evidence presented supporting extended periods of very shallow water deposition.

These observations also raise concern about an open marine origin for the Trezona Formation. Repetitive deepening cycles are not evident in the formation consistent with sea level change or parasequence formation, while a balanced position of shallow exposure surfaces is maintained from the paleosol at the base to the interbedded Yaltipena red bed sands at the top. The > 100m of sustained conditions supporting exposure is common to lake systems, but rare in marine systems where allocyclic controls like sea level change influence sediment grainsize and water depth.

The distribution of the Trezona Formation also supports a lacustrine origin. The Trezona Formation is not widespread like the Enorama Formation, rather isopachs of Trezona Formation shows it is limited to a bulls-eye pattern centred in the Central Flinders Ranges, and is likely influenced by synsedimentary deposition adjacent to salt diapir peripheral sinks (Lemon 1988). The association with alluvial sediments at the base and top of the Trezona, limited spatial distribution, covariation of C and O isotopes, and similarity to closed,

carbonate lake facies suggest that the Trezona isotopic anomaly may have more to do with lacustrine to very restricted marine conditions and provide a limited record of open ocean conditions. As such, it provides no constraint on the global carbon mass balance of carbon and the "Trezona Excursion" and is inappropriate as a correlation tool or global biogeochemical event.

Chemostratigraphic Correlation

The ability to correlate chemostratigraphic profiles within the Trezona Formation is key in determining whether the observed isotopic shift occurs synchronously across the entire basin at the time of deposition. For arguments of a primary oceanic isotopic signal to remain valid, chemostratigraphic profiles must be reproducible spatially within the formation and must be correlated with respect to time of deposition. Due to the lack of a laterally continuous marker bed in the Trezona Formation, any attempt to correlate measured stratigraphic sections must be tentative. Previous contributions have correlated distal sections within a basin using a δ13C datum, in the case of the Ombaatjie Formation in Namibia (Halverson *et al.* 2002), 0‰ VPDB. Sections with δ^{13}C values that do not fall below this datum are considered erosional and therefore incomplete (Halverson *et al.* 2002). This presents a circular argument with δ^{13}C value of 0‰ used to define a time line, and the global correlation of the isotope values based on the similarity of timing in a given basin of identical value. A comparison of the Blinman (Figure 9) and Emu Gap (Figure 8) sections reveals a facies dependence on δ^{13}C that is inconsistent with a globally changing δ^{13}C signal.

The Blinman and Emu Gap chemostratigraphic profiles share a common inflection point to more positive δ^{13}C values, broadly coincident with the transition to stacked stromatolite facies. McKirdy (2001) suggests that the inflection point is coincident with a shift to oolite

facies rather than stromatolite mounds, however, an oolite from the Trezona Range section (sample 27.4.11.63), returns a $\delta^{13}C$ value of -7.5‰ which not dissimilar to $\delta^{13}C$ values in the lower interval of the section, and Figures 3 and 4 suggest a coupling of positive $\delta^{13}C$ values with the stromatolitic facies. Thicknesses of stromatolite mound successions in the Blinman and Emu Gap sections are ~20m and ~160m respectively, with isotopic variation approaching $\delta^{13}C$ values of -3 in both sections. If the isotopic signal is assumed to reflect the primary marine signal at time of deposition, a common $\delta^{13}C$ end point would suggest that the isotope profiles presented here are complete and that the angle of inflection of $\delta^{13}C$ values is dependent on a deposition rate that was locally much faster. Alternatively, the large disparity in stromatolite thicknesses could be the result of erosion of the upper Trezona Formation in the Blinman section. The Blinman section records Elatina Formation diamictite directly overlying the upper Trezona stromatolite sequence. In a shelfal model for the Trezona, as proposed by Lemon (1988), the Yaltipena Formation should have been spatially distributed to the extent of the Trezona. The lack of Yaltipena Formation overlying the Trezona Formation in the Blinman section is indicative of a heavily eroded pre-Elatina succession. In this case, the isotope profile should be truncated in the upper Trezona depending on the scale of erosion. Therefore, the common end-point shared by the Blinman and Emu Gap sections is problematic if the Yaltipena is absent in the Blinman section but present in the Emu Gap section.

Nature of the Trezona Formation Isotopic Signal

Isotopic signals recorded in the Trezona Formation are used as a proxy for the carbon-oxygen isotopic composition of the Neoproterozoic at the time of lithification. The isotopic signal must be both primary and derived from a homogeneous marine environment for values to be representative of the ocean and to reflect the dynamics of global carbon

cycling. $\delta^{13}C$ and $\delta^{18}O$ compositions of the open ocean are seen to be controlled by discrete processes (organic productivity and climate respectively) and so any systematic relationship observed between these values will question their primary marine origin. The isotopic depletion associated with the Trezona Formation is widely considered to be primary (Singh 1986, Burgess 1999, McKirdy *et al.* 2001). A shelfal depositional environment for the Trezona Formation is assumed to record homogeneous marine values while the effects of diagenesis on $\delta^{13}C$ and $\delta^{18}O$ values are discounted, with claims that diagenetic cements are restricted to intraclastic and ooid facies and do not notably contribute to the observed isotopic excursion. Systematic patterns in isotopic profiles presented in this study may suggest a more complex origin for the steady-state depletion of $\delta^{13}C$ and $\delta^{18}O$ values observed in the lower Trezona Formation.

Isotopic variation in carbonates retaining primary marine values should only show stratigraphically-controlled trends, and should not display any systematic covariation of $\delta^{13}C$ and $\delta^{18}O$ values. The lower shale facies recognised in both the Blinman and Emu Gap stratigraphic sections records covariation of $\delta^{13}C$ and $\delta^{18}O$ values, both of which are significantly depleted. Covariation of $\delta^{13}C$ and $\delta^{18}O$ values is indicative of an origin that is intimately linked, which is difficult to resolve in a homogeneous oceanic environment. The Emu Gap section also records second-order variability contributing to a broader trend towards lighter isotopic values (Figure 10). While meteoric input into a restricted marine or lacustrine environment could potentially cause stepwise depletion of $\delta^{18}O$ of the observed magnitude, a diagenetic origin for covariant depletion in the lower Trezona Formation is supported by this study. Diagenetic cements and concretions occur in abundance in the lower shale facies, and hence a facies association with depletion of $\delta^{13}C$ and $\delta^{18}O$ values is

evident. Extreme covariation observed in a highly isotopically variable concreted shale interval (Figure 13a, b) is indicative of mixing of different carbonate phases suggesting that a pore fluid-mixing origin for the second-order pattern of variation is likely. Systematic isotopic patterns and lithological associations in the lower Trezona Formation are typical of meteoric diagenetic processes (Swart & Kennedy 2011) and show little evidence of primary marine values.

The middle interval of the Trezona Formation in the Emu Gap section is associated with a succession of interbedded flakestone breccia and microbial laminite beds and preserves no clear association between $\delta^{18}O$ and $\delta^{13}C$. While systematic relationships between $\delta^{18}O$ and $\delta^{13}C$ are lacking in this interval, values are still highly depleted, with $\delta^{13}C$ values persisting below mantle levels (Melezhik *et al.* 2005), and cannot be resolved by a normal marine environment. It could be speculated that lithological change in this interval (marked by the disappearance of concretionary shales) is reflected in the isotopic profile, however this relationship is tenuous.

The upper stromatolite facies in both the Emu Gap and Blinman sections records divergent $\delta^{13}C$ and $\delta^{18}O$ values. Variation in $\delta^{13}C$ and $\delta^{18}O$ appears related, producing a negative correlation when cross-plotted in the Emu Gap section (Figure 12), and shows no diagnostic evidence of a diagenetic mechanism. A sharp inflection towards lighter $\delta^{13}C$ value coincident with the abrupt shift to stromatolites in the Blinman section is indicative of a strong facies association (Figure 9). The large discrepancy in thicknesses of upper stromatolite intervals likely reflects either the rate of deposition or truncation by erosion prior to the deposition of the overlying Elatina Formation. Similarity in the maximum observed $\delta^{13}C$ values is problematic for an erosional control on stromatolite thickness suggesting an environmental

control is more likely, however the exact mechanism responsible for isotopic divergence in the upper Trezona remains ambiguous. A primary origin of isotopic variation here would preclude an unperturbed marine interpretation due to extreme depletion of $\delta^{18}O$ values. The lack of a reproducible signal describing $\delta^{18}O$ depletion also implies that a pervasive mechanism driving isotopic divergence is unlikely. Environmental variation, likely deepening indicated by the lack of preserved evidence of desiccation in the upper Trezona interval, related to the dominance of stromatolite growth is therefore the most plausible alternative.

CONCLUSION

Despite high magnitude, negative $\delta^{13}C$ shifts associated with the "Trezona Anomaly" being widely interpreted to record primary marine variation, the results of this study indicates that isotopic variation in the Trezona Formation may have a more complex origin. Field observations question previous interpretations of the Trezona Formation as a first-order shallowing-up from the shelfal muds of the Enorama Shale. A paleosol at Bulls Gap representing a sequence boundary at the base of the Trezona Formation defines it as its own discrete depositional cycle and suggests exposure for a period of time long enough to develop a soil horizon. Furthermore, consistent desiccation cracks preserved in the lower half of the Trezona are suggestive of an extended period of extremely shallow-water conditions, coincident with isotopic depletion correlated with the Trezona Anomaly globally. When considered with the spatial restriction of the Trezona Formation, these observations suggest that an open, shelfal depositional environment is unlikely to be responsible for the Trezona Formation. Closed-marine or lacustrine deposition may have deposited the Trezona Formation. While the exact mechanisms controlling isotopic depletion and variation in the Trezona Formation remain ambiguous, several lines of evidence indicate that a primary

marine isotopic signal is unlikely to be recorded in the Trezona. First-order covariant positive and negative relationships are recorded confined to lithological intervals, indicating isotopic patterns are not open marine in nature, and are likely diagenetically and environmentally controlled in the lower and upper Trezona Formation respectively. A non-primary marine origin for the "Trezona Anomaly" signal implies that it is not representative of the carbon-oxygen isotope chemistry of the pre-Marinoan glacial ocean, rather it records common alteration of coastal or lacustrine carbonates responding to eustatic change leading up to the Marinoan glaciation.

ACKNOWLEDGEMENTS

FIGURE CAPTIONS

Figure 1. (a) Geological map of the Central Flinders Ranges. Measured section locations are marked with coloured circles. The Australia map inset locates the Adelaide Fold-Thrust Belt in red and the central Flinders Ranges study area in the black rectangle. (b) Summary of the Umberatana Group stratigraphy, Central Flinders Ranges (after Lemon, 1988)

Figure 2. Distribution map of the Trezona Formation.

Figure 3. Photographs of sedimentary and dissolution features in the Trezona Formation sediments. (a) Resistant bed in the shale facies preserving ripple cross-laminations in the Trezona Range section; (b) Stacking pattern of micritic flake intraclasts in the flakestone breccia facies, Trezona Range. Flakes are orientated both parallel and perpendicular to the bedding plane, suggesting high-energy storm event deposition; (c) Mudcracks preserved in the lower Little Bunkers Range section. These mudcracks are preserved in a 2cm thick marl layer overlying a flakestone breccia bed; (d) Styolite cross-cutting an intraclastic grainstone bed, indicating pressure dissolution. Trezona Range; (e) Well-formed cumulate stromatolite domes, Little Bunkers Range.(f) Cumulate stromatolite domes overlying redbed sandstone beds, Trezona Range. Stromatolites contour to a channelised sandstone surface; (g) Stacked microbial laminites, Little Bunkers Range; (h) Paleokarst-infilling collapse conglomerate from the upper contact between the Trezona Formation and the Yaltipena Formation in the Trezona Range section.

Figure 4. Measured stratigraphic section of the Trezona Formation in the Trezona Range.

Figure 5. Measured stratigraphic section of the Trezona Formation in the Little Bunkers Range.

Figure 6. (a) Photograph of an intraclastic breccia hosting the possible animal body fossils of Maloof et al. (2010) Internal layering is defined by sandy drapes. Little Bunkers Range; (b) Stacking pattern of an intraclastic breccia (with "body fossils"). Little Bunkers Range; (c) Micropictograph of a recrystallised "body fossil" clast in an intraclastic breccia, Little Bunkers Range (sample 1.5.11.7). A micritic matrix is supporting a microspar-pseudospar replaced clast. Clast crystals coursen to ~1mm in width towards the clast interior.; (d) Micropictograph of a recrystallised "body fossil" clast in an intraclastic breccia, Little Bunkers Range (sample 1.5.11.7). A dog-tooth spar has formed along the interior of the clast margin after dissolution. Reprecipitation of clast-filling sparry mosaic post-dates marginal precipitation and concentrates insoluble material along the clast margin.

Figure 7. Photos of basal contacts in the Trezona Range, Trezona Formation. (a) Enorama Creek contact. The unconformable surface defining the contact (dashed line) is the interface between the upper Enorama Shale (green) and the lower surface of Trezona Formation cumulate stromatolite domes (blue); (b) Bulls Gap contact. Enorama Shale beds (green) overlain by fine sand with mudcracks in silty drapes. The contact is denoted by a dashed line. ; (c) Weathering horizon at the Trezona Formation contact with the Enorama Shale, preserving in-situ weathered shale derived from the underlying Enorama Shale.

Figure 8. Stratigraphic section of the Trezona Formation at Emu Gap (after Maloof *et al*. 2010) with $\delta^{13}C$ and $\delta^{18}O$ isotopic profiles plotted against stratigraphic height. Closed diamonds represent $\delta^{13}C$ VPDB, open squares represent $\delta^{18}O$ VPDB.

Figure 9. Stratigraphic section of the Trezona Formation at Blinman (Martin Kennedy pers comms.) with δ^{13}C and δ^{18}O isotopic profiles plotted against stratigraphic height. Closed diamonds represent δ^{13}C VPDB, open squares represent δ^{18}O VPDB.

Figure 10. δ^{13}C VPDB plotted against stratigraphic height over the 170-230 m interval of the Emu Gap section (after Maloof *et al*. 2010) recording second order variation and cyclicity within a first order trend of increasingly positive isotope values.

Figure 11. δ^{18}O VPDB plotted against stratigraphic height over the 40-100 m interval of the Emu Gap section (after Maloof *et al*. 2010) recording second order variation and cyclicity within a first order trend of increasingly positive isotope values.

Figure 12. Cross-plot of δ^{13}C VPDB versus δ^{18}O VPDB in the Emu Gap section (after Maloof *et al*. 2010). Systematic trends associated with facies changes are recognised. A) represents values showing a positive relationship between contiguous samples of the same lithology, suggesting a second order step-wise variation. Similarly, B) represents a negative relationship between contiguous samples of the same lithology (stromatolites) varying in a step-wise fashion.

Figure 13. (a) Plot of isotopic variation preserved in the lower Trezona Formation interval. Closed diamonds represents δ^{13}C values, open squares represent δ^{18}O values. (b) Describes the covariant relationship between δ^{13}C and δ^{18}O values.

Figure 14. Micropictographs of diagenetic textures in the Trezona Formation. (a) Flakestone breccia (sample 26.4.11.7) showing micritic matrix-supported flake-clasts with selective recrystallisation to blocky spar in clast interiors. (b) Flakestone breccia preserves later-stage styolites. (c) Intraclastic grainstone (sample 27.4.11.83) preserving micritic rims nucleated around intraclasts. Clast interiors have been selectively recrystallised with relict rims preserving the original clast shape. (d) Intraclastic grainstone (sample 27.4.11.44) with Fe-calcite spar (blue stain) isopachous fringing cements. Clast interiors and pore-filling cements appear to lack Fe-calcite. (e) Oolite (sample 30.4.11.55) preserving a single microspar phase. Relict intraclast (ooid) shape is preserved in remnant insoluble material. (f) Oolie (sample 30.4.11.92) with ooid intraclasts preserving varying degrees of recrystallisation and truncation by styolites.

REFERENCES

BJERRUM C. J. & CANFIELD D. E. 2011. Towards a quantitative understanding of the late Neoproterozoic carbon cycle. *Proceedings of the National Academy of Sciences of the United States of America* **108**, 5542-5547.

BURGESS J. M. 1999. Carbon isotope stratigraphy of the interglacial Umberatana Group, Adelaide fold Belt, South Australia. Ph.D. thesis, Department of Geology and Geophysics, The University of Adelaide, Adelaide (unpubl.).

CHRISTIE-BLICK N., SOHL L. E. & KENNEDY M. J. 1999. Considering a Neoproterozoic snowball earth. *Science* **284**, 1087.

COMPTON R. R. 1985. *Geology in the field*. John Wiley & Sons.

DERRY L. A. 2010. A burial diagenesis origin for the Ediacaran Shuram-Wonoka carbon isotope anomaly. *Earth and Planetary Science Letters* **294**, 152-162.

DICKSON J. 1965. A modified staining technique for carbonates in thin section.

FIKE D. A., GROTZINGER J. P., PRATT L. M. & SUMMONS R. E. 2006. Oxidation of the Ediacaran Ocean. *Nature* **444**, 744-747.

GROTZINGER J. P., FIKE D. A. & FISCHER W. W. 2011. Enigmatic origin of the largest-known carbon isotope excursion in Earth's history. *Nature Geoscience* **4**, 285-292.

HALVERSON G. P., HOFFMAN P. F., SCHRAG D. P. & KAUFMAN A. J. 2002. A major perturbation of the carbon cycle before the Ghaub glaciation (Neoproterozoic) in Namibia: Prelude to snowball Earth? *Geochemistry Geophysics Geosystems* **3**.

HALVERSON G. P., HOFFMAN P. F., SCHRAG D. P., MALOOF A. C. & RICE A. H. N. 2005. Toward a Neoproterozoic composite carbon-isotope record. *Geological Society of America Bulletin* **117**, 1181-1207.

HOFFMAN P. F., HALVERSON G. P. & GROTZINGER J. P. 2002. Are Proterozoic cap carbonates and isotopic excursions a record of gas hydrate destabilization following Earth's coldest intervals?: Comment. *Geology* **30**, 286-287.

HOFFMAN P. F., KAUFMAN A. J., HALVERSON G. P. & SCHRAG D. P. 1998. A Neoproterozoic snowball earth. *Science* **281**, 1342-1346.

KENNEDY M., MROFKA D. & VON DER BORCH C. 2008. Snowball Earth termination by destabilization of equatorial permafrost methane clathrate. *Nature* **453**, 642-645.

KNAUTH L. P. & KENNEDY M. J. 2009. The late Precambrian greening of the Earth. *Nature* **460**, 728-732.

LE GUERROUE E., ALLEN P. A., COZZI A., ETIENNE J. L. & FANNING M. 2006. 50 Myr recovery from the largest negative delta C-13 excursion in the Ediacaran ocean. *Terra Nova* **18**, 147-153.

LEMON N. & REID P. 1998. The Yaltipena Formation of the central Flinders Ranges. *MESA Journal* **8**, 37-39.

LEMON N. M. 1988. Diapir recognition and modelling with examples from the late Proterozoic Adelaide Geosyncline, central Flinders Ranges, South Australia. Ph.D thesis, Department of Geology and Geophysics, The University of Adelaide (unpubl.).

MALOOF A. C., ROSE C. V., BEACH R., SAMUELS B. M., CALMET C. C., ERWIN D. H., POIRIER G. R., YAO N. & SIMONS F. J. 2010. Possible animal-body fossils in pre-Marinoan limestones from South Australia. *Nature Geoscience* **3**, 653-659.

MCFADDEN K. A., HUANG J., CHU X., JIANG G., KAUFMAN A. J., ZHOU C., YUAN X. & XIAO S. 2008. Pulsed oxidation and biological evolution in the Ediacaran Doushantuo Formation. *Proceedings of the National Academy of Sciences* **105**, 3197.

MCKIRDY D. M., BURGESS J. M., LEMON N. M., YU X. K., COOPER A. M., GOSTIN V. A., JENKINS R. J. F. & BOTH R. A. 2001. A chemostratigraphic overview of the late Cryogenian interglacial sequence in the Adelaide Fold-Thrust Belt, South Australia. *Precambrian Research* **106**, 149-186.

MELEZHIK V. A., FALLICK A. E. & POKROVSKY B. G. 2005. Enigmatic nature of thick sedimentary carbonates depleted in C-13 beyond the canonical mantle value: The challenges to our understanding of the terrestrial carbon cycle. *Precambrian Research* **137**, 131-165.

PREISS W. V. 1996. New members of the Waukaringa Siltstone. *MESA Journal* **1**, 40-45.

PREISS W. V. 2000. The Adelaide Geosyncline of South Australia and its significance in Neoproterozoic continental reconstruction. *Precambrian Research* **100**, 21-63.

PREISS W. V. C. 1987. *The Adelaide Geosyncline-late Proterozoic stratigraphy, sedimentation, palaeontology and tectonics.* (Vol. 53). Bull. geol. Surv. S. Aust.

RAISWELL R. & FISHER Q. 2000. Mudrock-hosted carbonate concretions: a review of growth mechanisms and their influence on chemical and isotopic composition. *Journal of the Geological Society* **157**, 239.

SCHRAG D. P., BERNER R. A., HOFFMAN P. F. & HALVERSON G. P. 2002. On the initiation of a snowball Earth. *Geochemistry Geophysics Geosystems* **3**.

SINGH U. 1986. Late precambrian and Cambrian carbonates of the Adelaidean in the Flinders Ranges, South Australia - A petrographic, electron microprobe and stable isotope study. Ph.D. thesis, Department of Geology and Geophysics, University of Adelaide, Adelaide (unpubl.).

SWART P. K. 2008. Global synchronous changes in the carbon isotopic composition of carbonate sediments unrelated to changes in the global carbon cycle. *Proceedings of the National Academy of Sciences of the United States of America* **105**, 13741-13745.

SWART P. K. & KENNEDY M. J. 2011. Does the Global Stratigraphic Reproducibility of δ^{13}C in Neoproterozoic Carbonates Require a Marine Origin? A Plio-Pleistocene Comparison. *Geology*.

TZIPERMAN E., HALEVY I., JOHNSTON D. T., KNOLL A. H. & SCHRAG D. P. 2011. Biologically induced initiation of Neoproterozoic snowball-Earth events. *Proceedings of the National Academy of Sciences of the United States of America* **108**, 15091-15096.

VEIZER J., ALA D., AZMY K., BRUCKSCHEN P., BUHL D., BRUHN F., CARDEN G. A. F., DIENER A., EBNETH S., GODDERIS Y., JASPER T., KORTE C., PAWELLEK F., PODLAHA O. G. & STRAUSS H. 1999. Sr-87/Sr-86, delta C-13 and delta O-18 evolution of Phanerozoic seawater. *Chemical Geology* **161**, 59-88.

WILLIAMS G. E., GOSTIN V. A., MCKIRDY D. M. & PREISS W. V. 2008. The Elatina glaciation, late Cryogenian (Marinoan Epoch), South Australia: Sedimentary facies and palaeoenvironments. *Precambrian Research* **163**, 307-331.
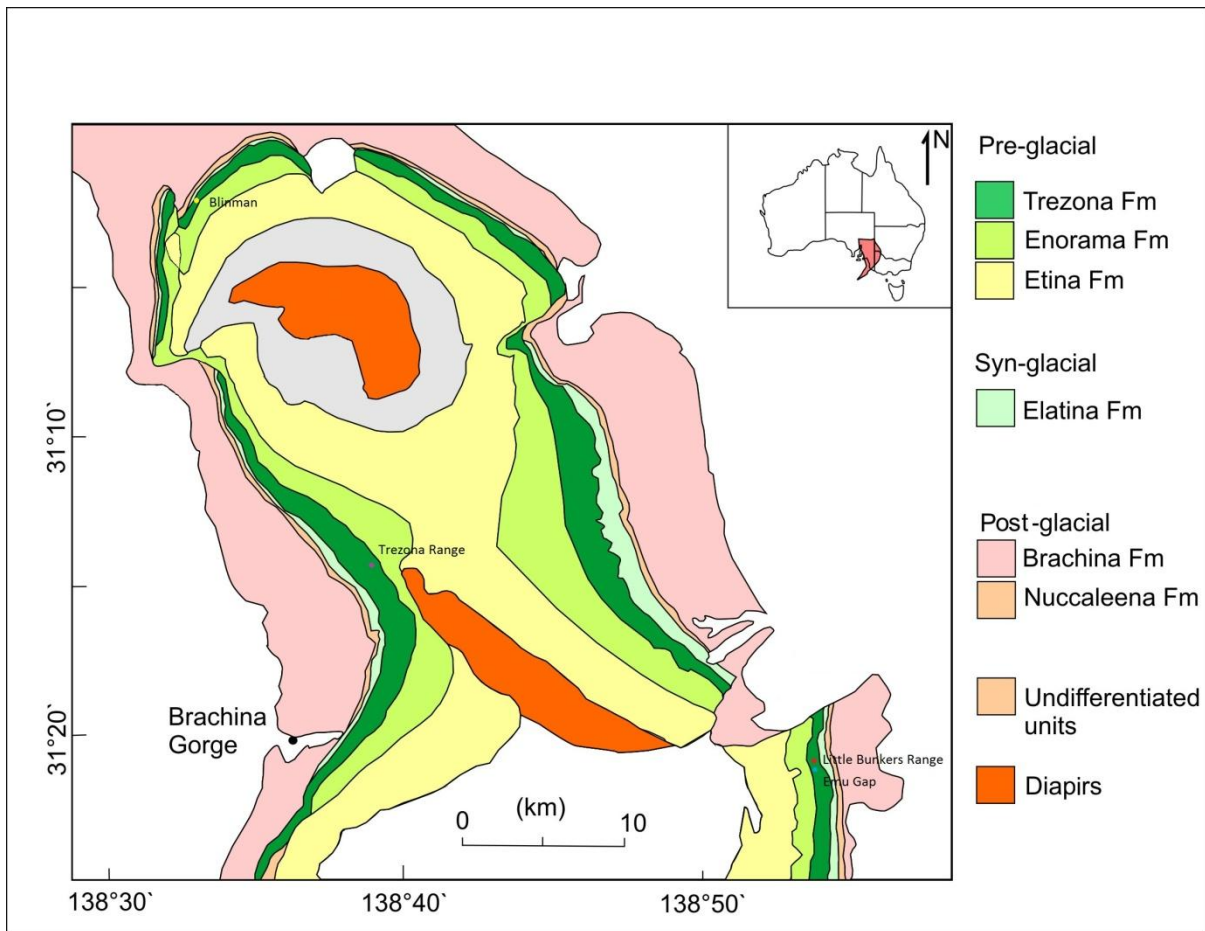
Figure 1a: above Figure1b (below)
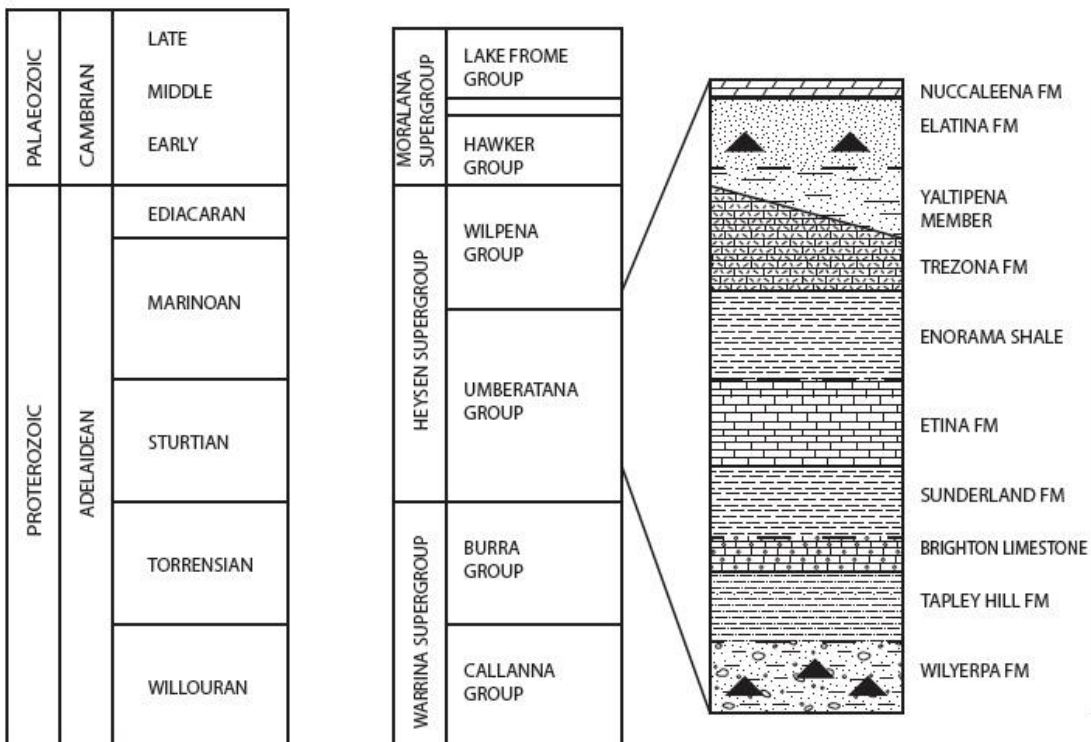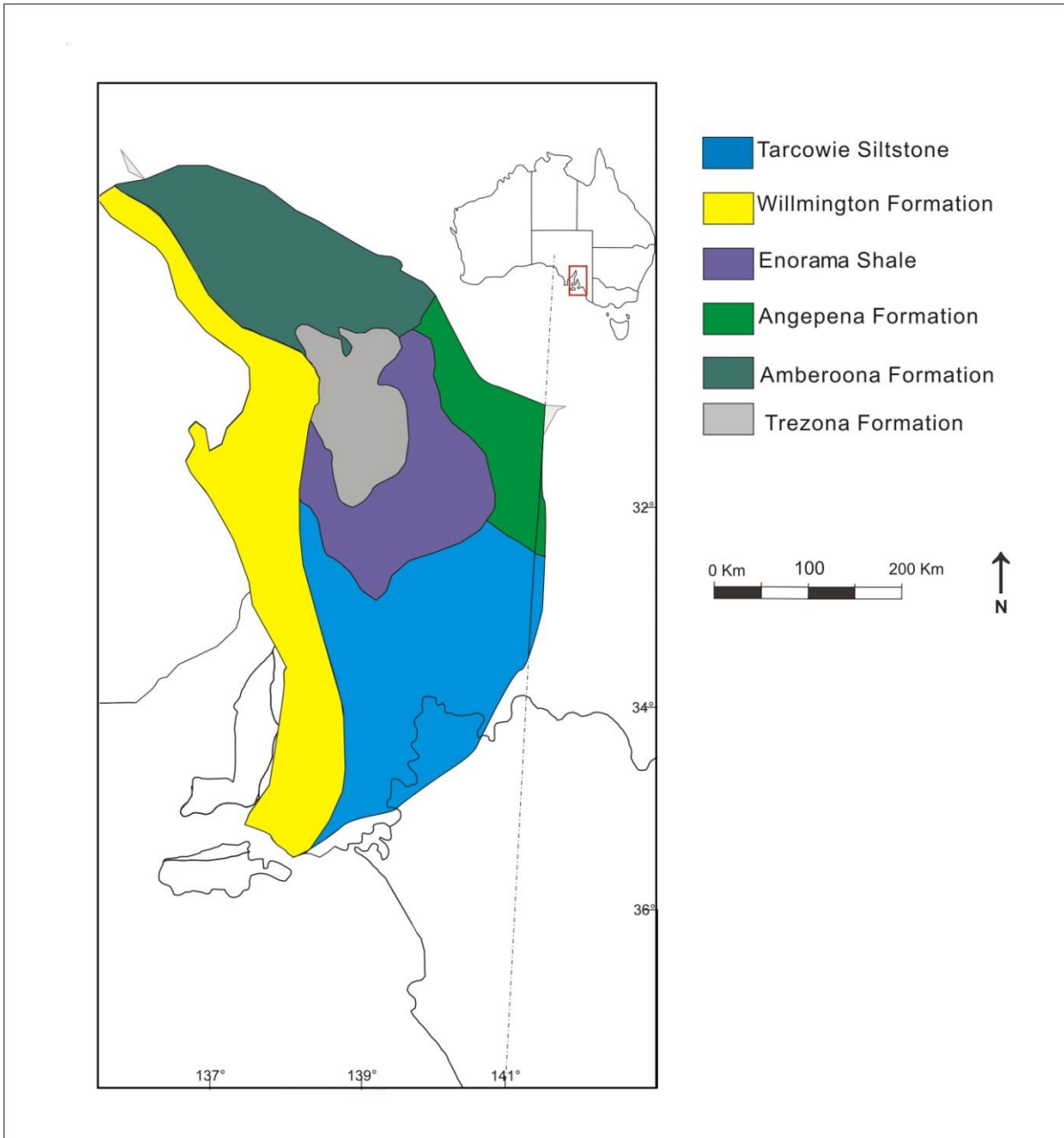
Figure 2
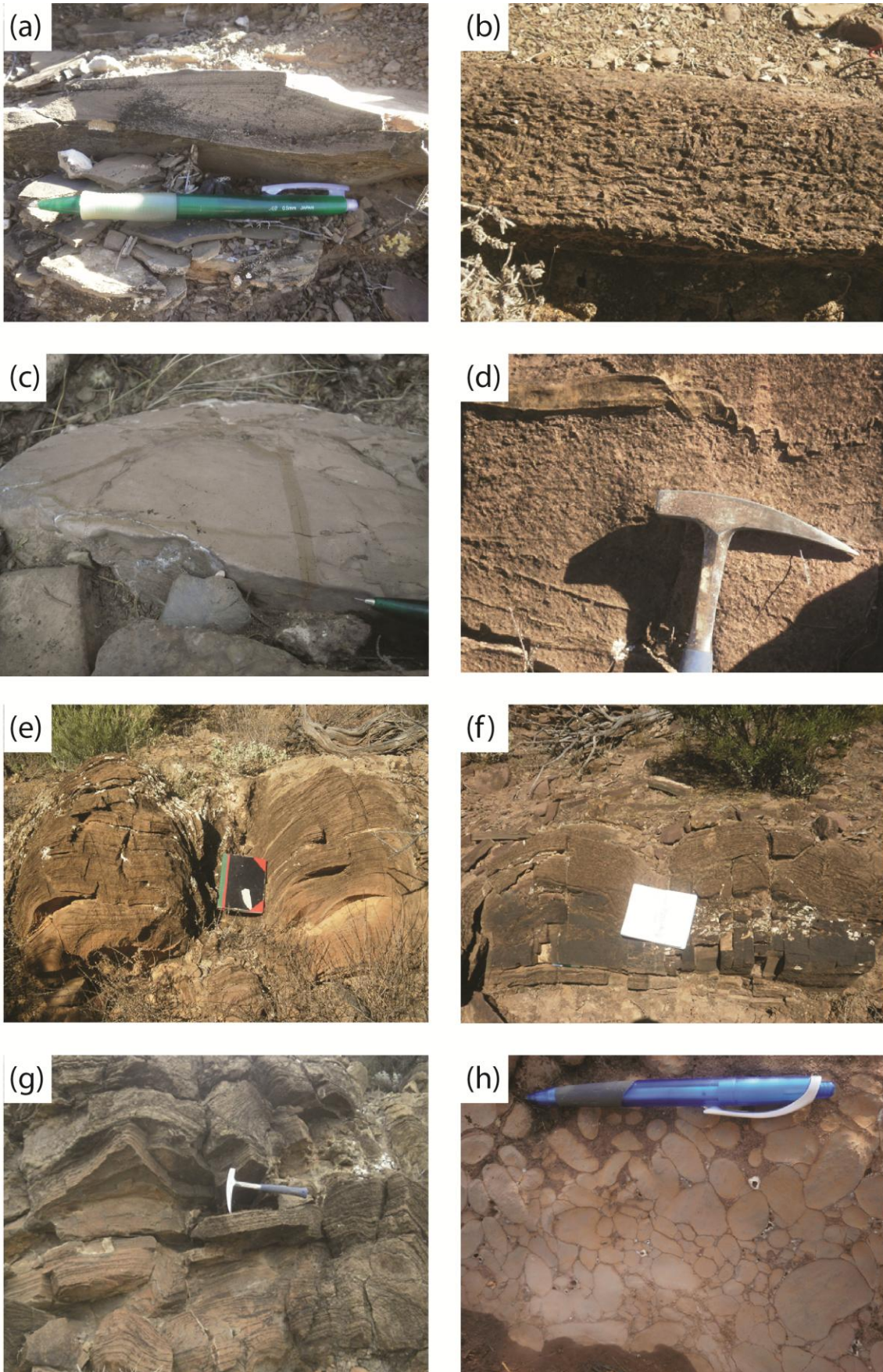
Figure 3
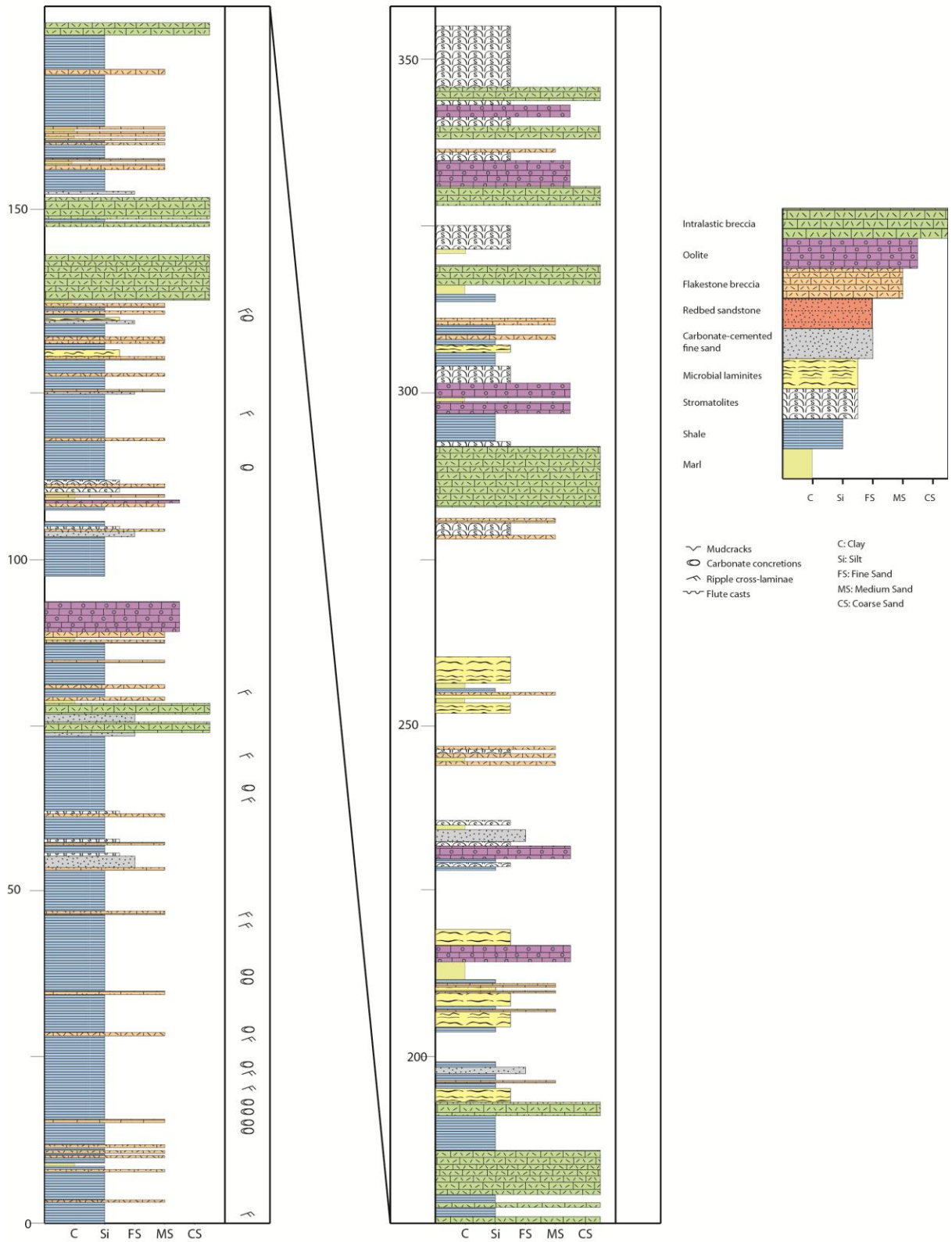
Figure 4
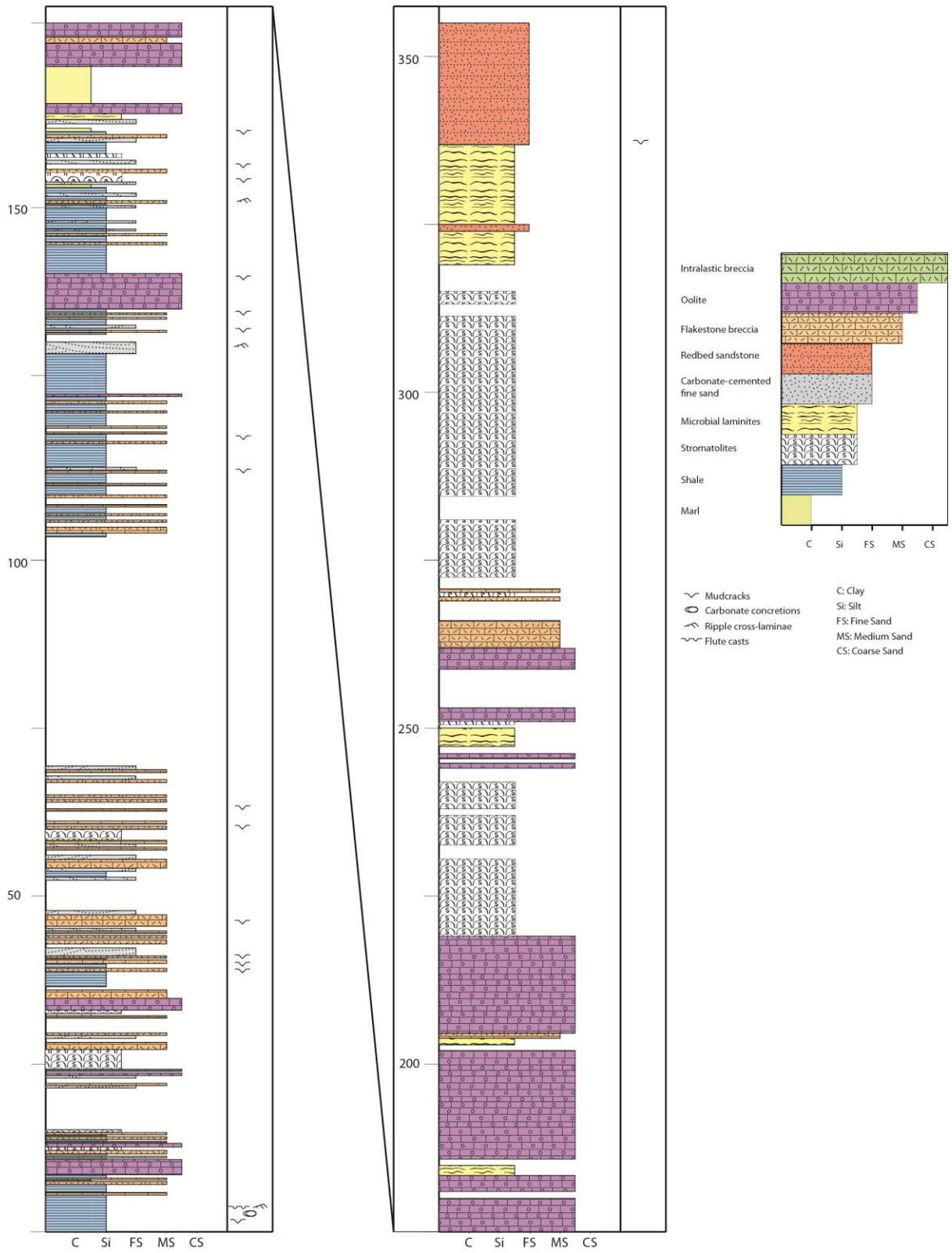
Figure 5
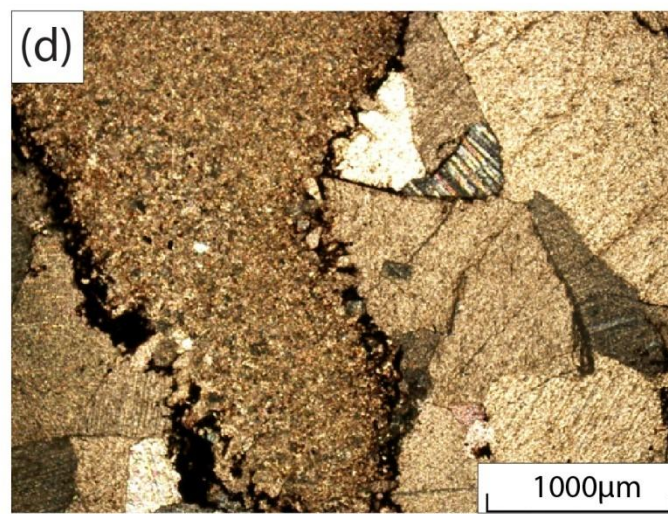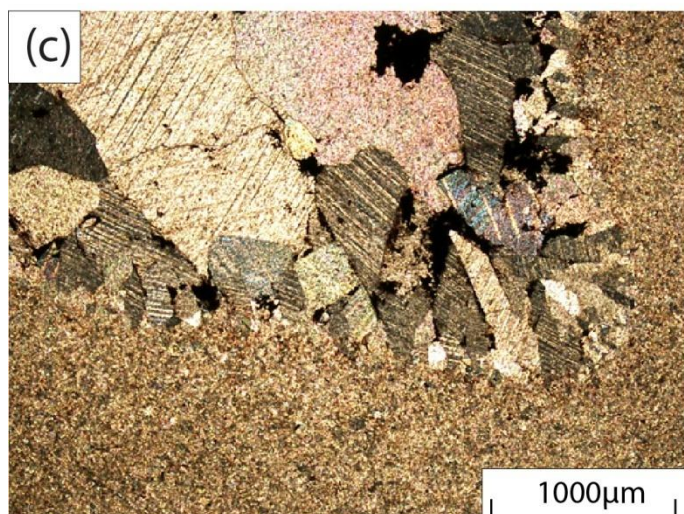
Figure 6
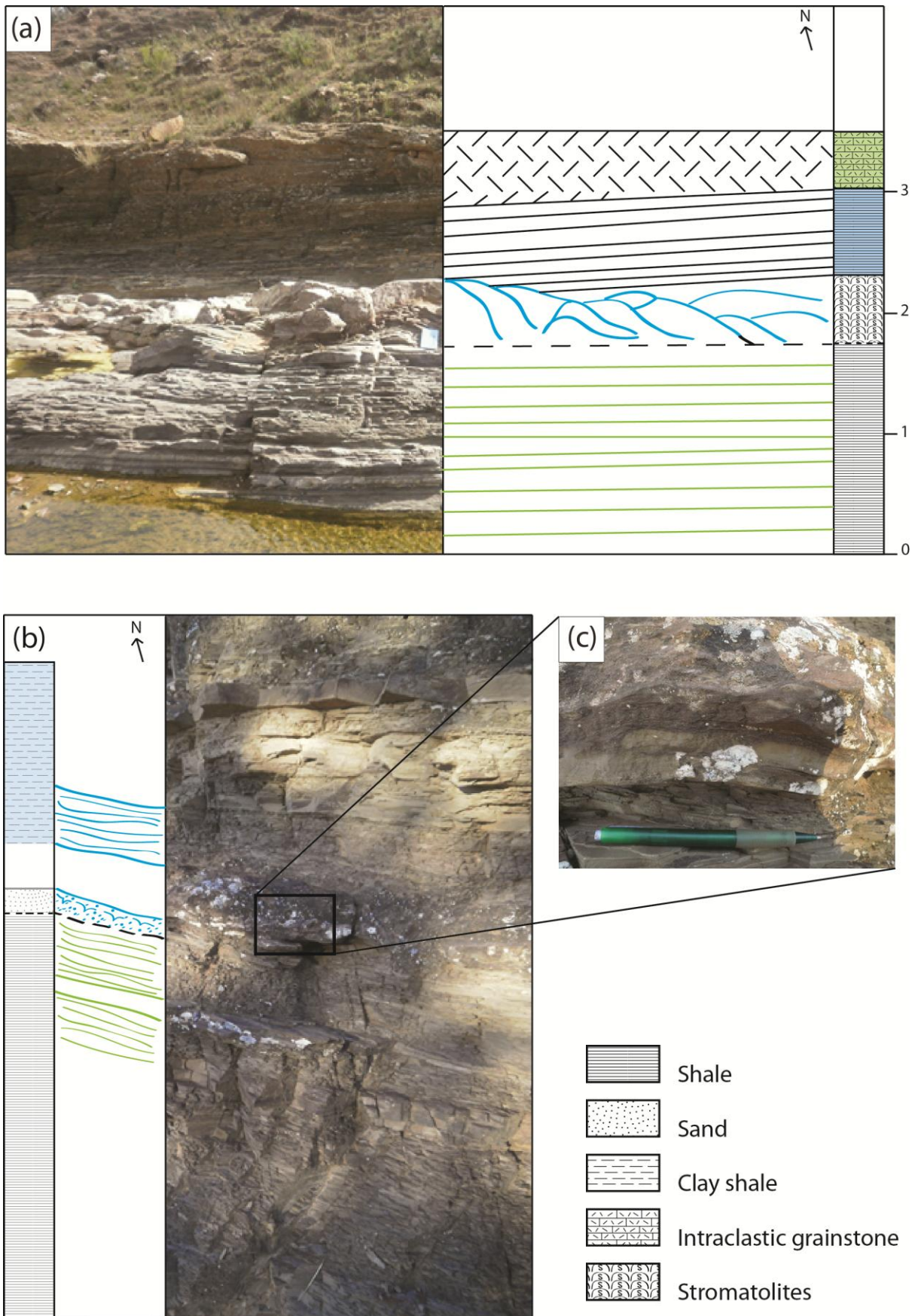
Figure 7
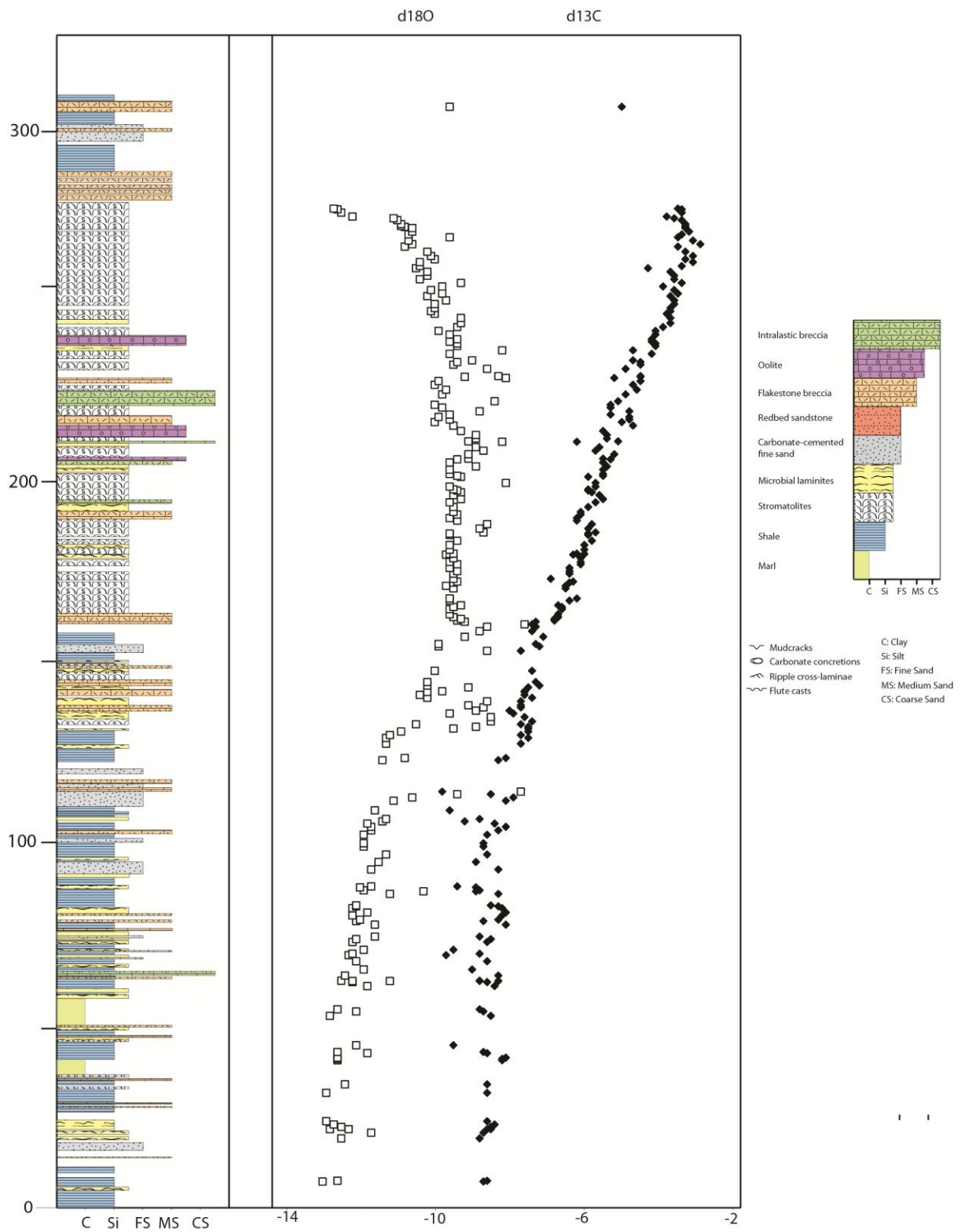
Figure 8
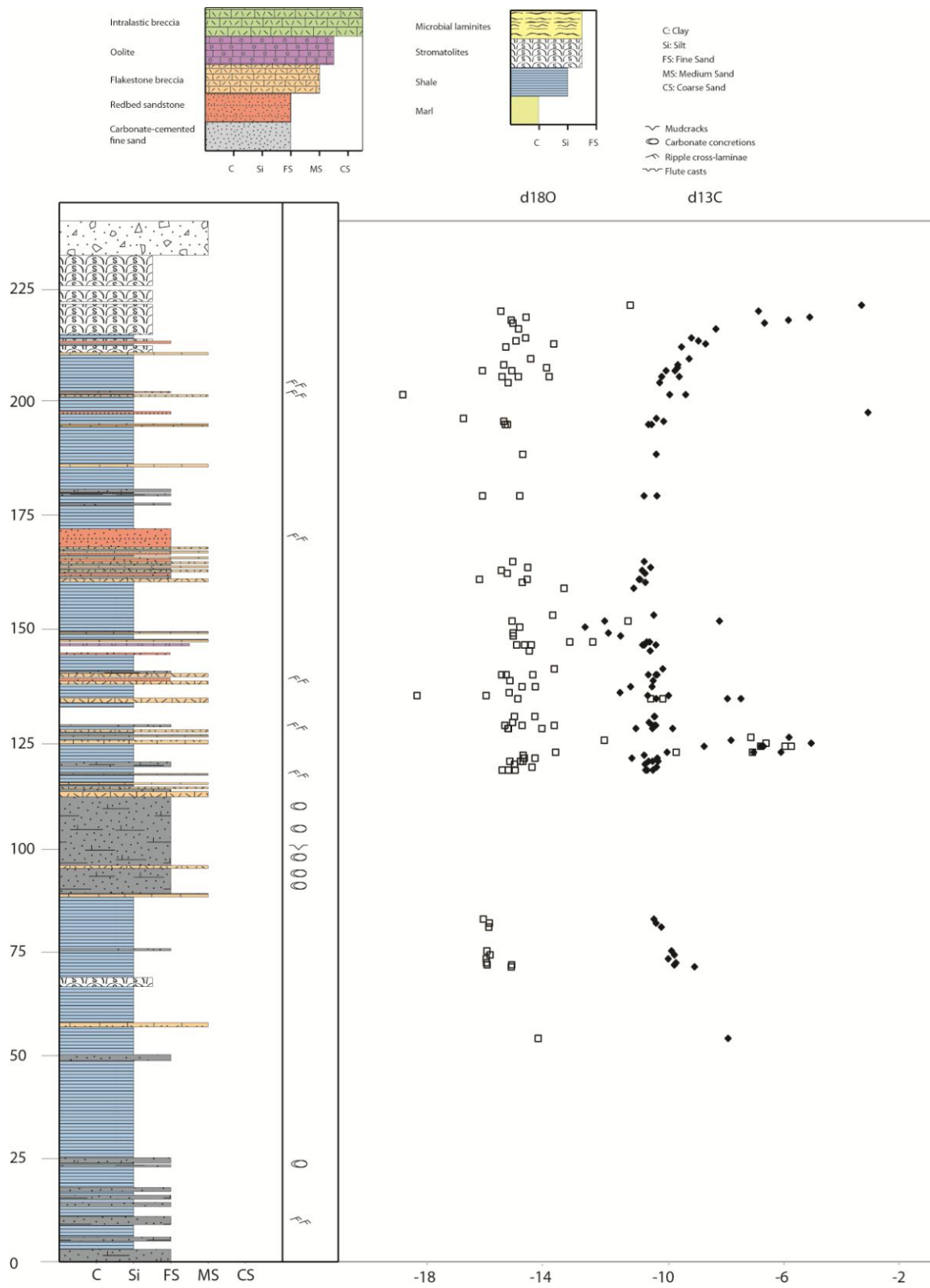
Figure 9
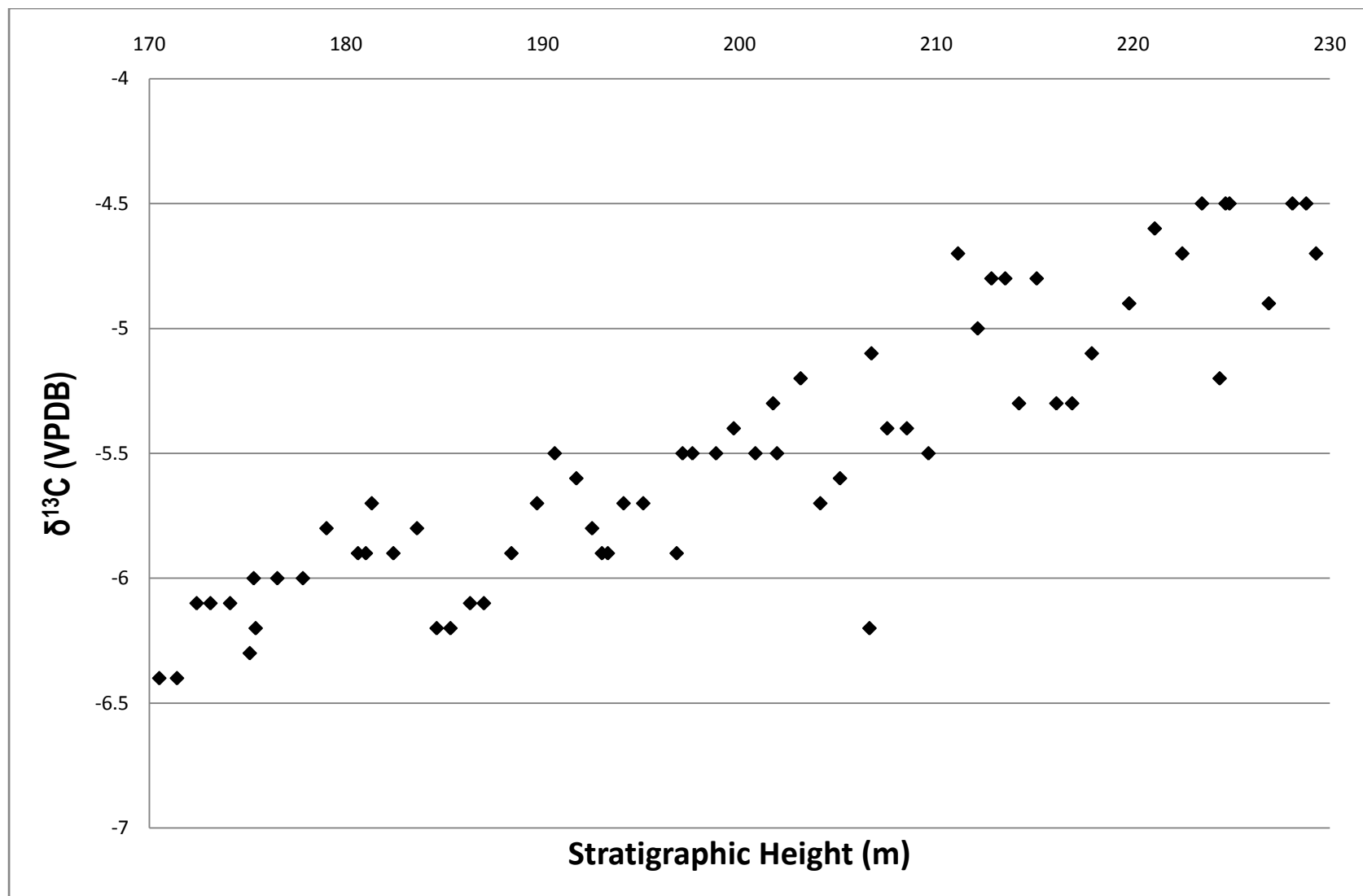
Figure 10
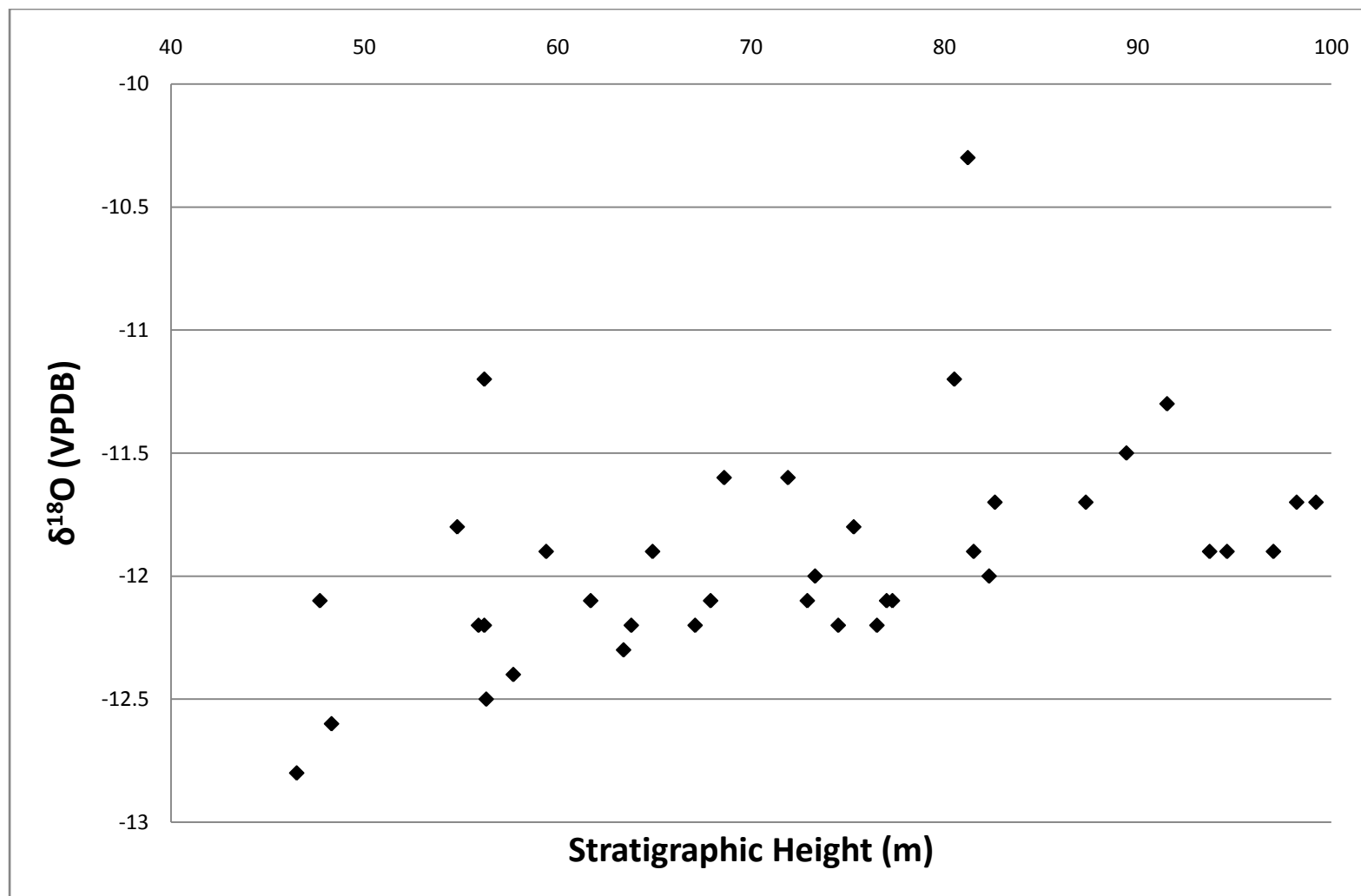
Figure 11
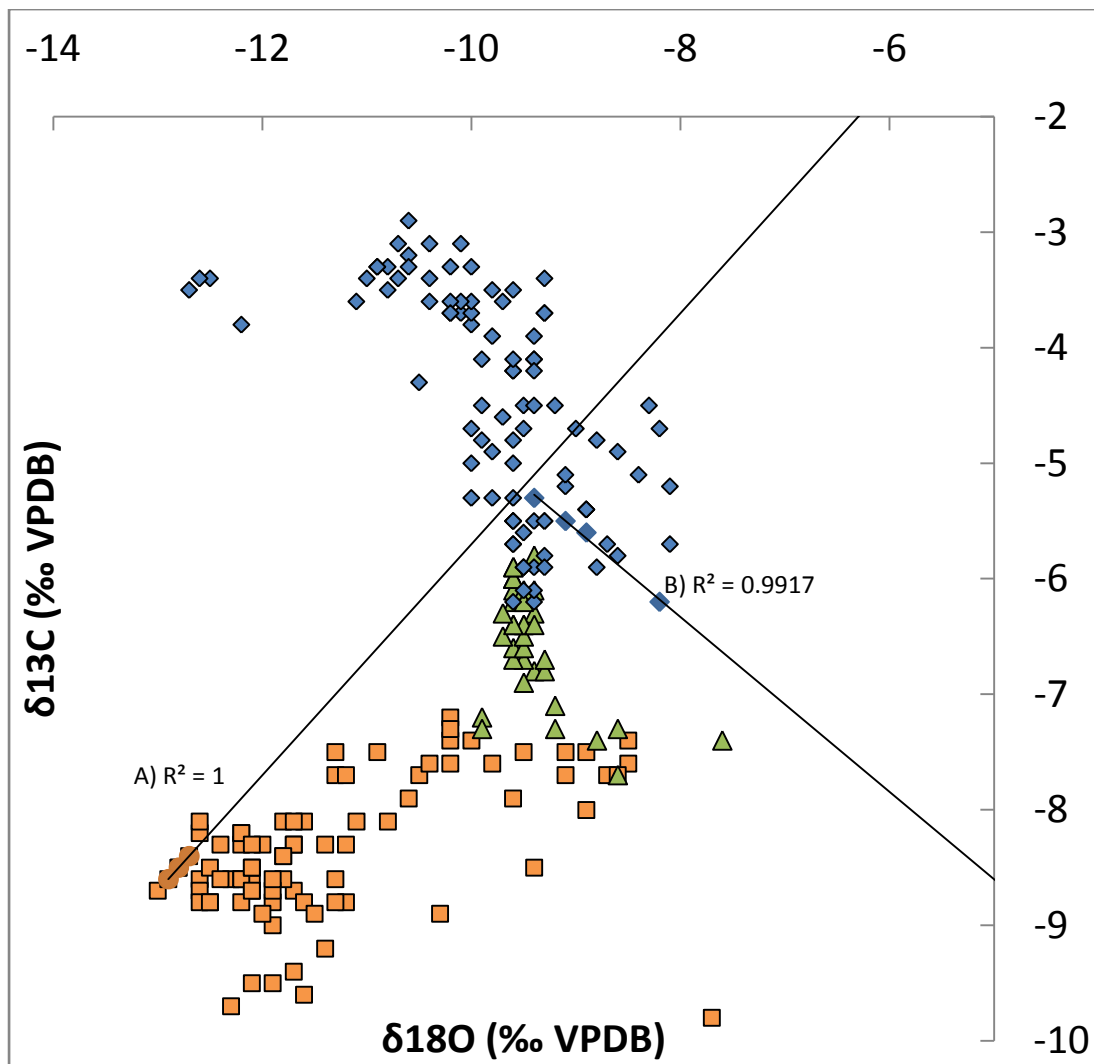
**Figure 12**
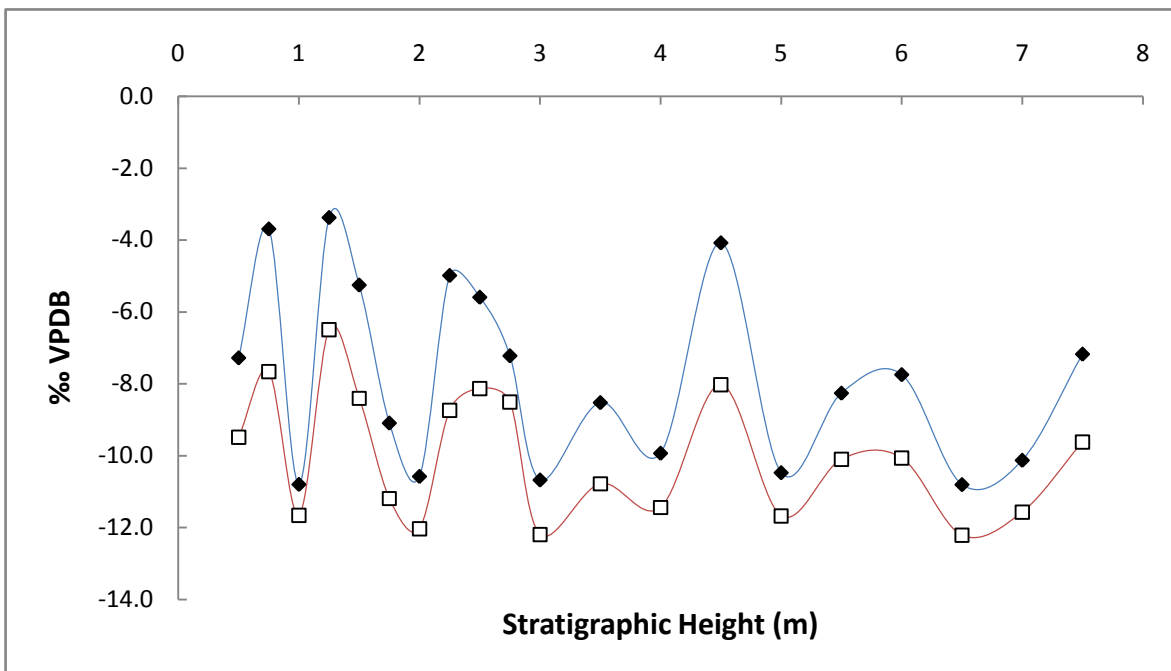
**Figure 13a: (above) Figure 2b (below)**
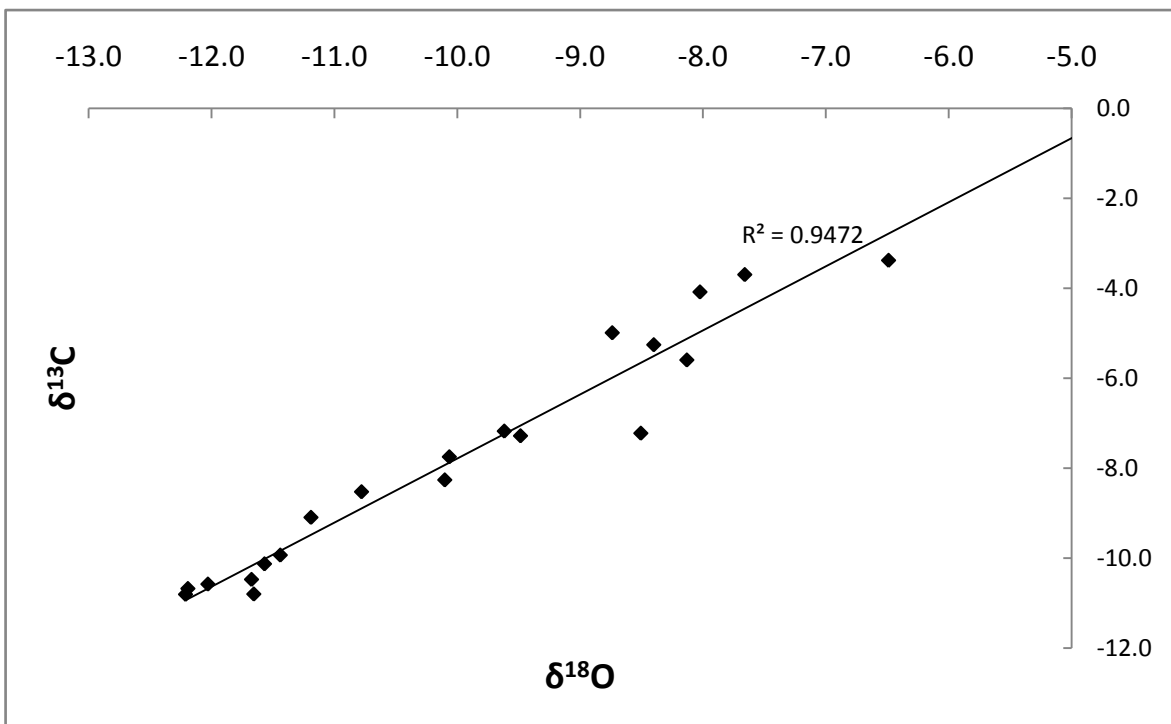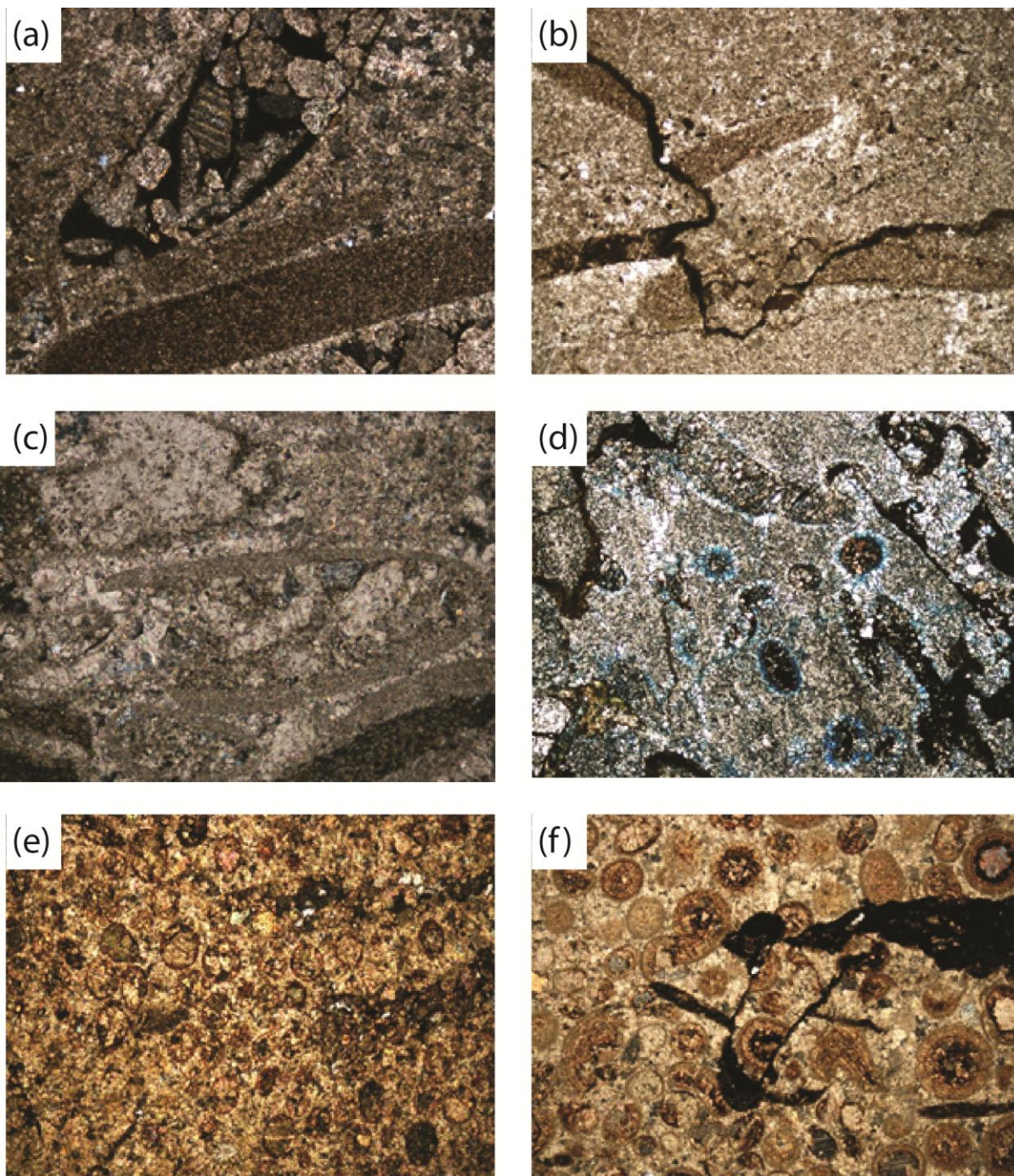
Figure 14

LIST OF APPENDICES

1. **SAMPLE LIST**
   a. **Blinman**
   b. **Trezona Range**
   c. **Little Bunkers Range**

2. **RAW STABLE ISOTOPE DATA**
   a. **2.1 Blinman**
   b. **2.2 Emu Gap (Maloof et al. 2010)**

3. **THIN-SECTION DESCRIPTIONS**
   a. **3.1 Trezona Range**
   b. **3.2 Little Bunkers Range**

1.1 Blinman

Sample Series	Sample #	Stratigraphic Height (m)	Lithology	Analysis
31.10.10	3	66		HS
31.10.10	4	66.5		HS
31.10.10	5	67		HS
31.10.10	6	68		HS
31.10.10	7	69		HS
31.10.10	8	70		HS
31.10.10	12	48		HS
31.10.10	14	76		HS
31.10.10	15	77		HS
31.10.10	17	78		HS
31.10.10	18	79		HS
31.10.10	19	80		HS
31.10.10	20	80.5		HS
31.10.10	21	81		HS
31.10.10	22	81.25		HS
31.10.10	23	81.5		HS
1.11.10	1	115.5	Flakestone Breccia	HS
1.11.10	2	116.25	Flakestone Breccia	HS
1.11.10	3	117	Flakestone Breccia	HS
1.11.10	4	117.75	Flakestone Breccia	HS
1.11.10	5	117.75	Flakestone Breccia	HS
1.11.10	6	118.5	Carb. Cemented Fine Sand	HS
1.11.10	7	118.5	Carb. Cemented Fine Sand	HS
1.11.10	8	119.25	Carb. Cemented Fine Sand	HS
1.11.10	9	120	Shale	HS
1.11.10	10	120	Shale	HS
1.11.10	11	120	Carb. Cemented Fine Sand	HS
1.11.10	12	121.5	Carb. Cemented Fine Sand	HS
1.11.10	13	121.5	calcite vein	HS
1.11.10	14	122.25	Shale	HS
1.11.10	15	123	Shale	HS
1.11.10	16	123.75	Marl	HS
1.11.10	17	126	Flakestone Breccia	HS
1.11.10	18	126	Marl	HS
1.11.10	19	126.75	Flakestone Breccia	HS
1.11.10	20	126.75	Flakestone Breccia	HS
1.11.10	21	127.5	Flakestone Breccia	HS
1.11.10	22	129	Carb. Cemented Fine Sand	HS
1.11.10	23	133.5	Carb. Cemented Fine Sand	HS
1.11.10	24	133.5	Carb. Cemented Fine Sand	HS
1.11.10	25	133.5	Flakestone Breccia	HS

1.11.10	26	134.25	Flakestone Breccia	HS
1.11.10	27	135	Carb. Cemented Fine Sand	HS
1.11.10	28	136.5	Carb. Cemented Fine Sand	HS
1.11.10	29	136.5	Shale	HS
1.11.10	30	138	Flakestone Breccia	HS
1.11.10	31	139.5	Flakestone Breccia	HS
1.11.10	32	139.5	Carb. Cemented Fine Sand	HS
1.11.10	33	139.5	Flakestone Breccia	HS
1.11.10	34	141	Carb. Cemented Fine Sand	HS
1.11.10	37	145.5	Carb. Cemented Fine Sand	HS
1.11.10	38	147	Carb. Cemented Fine Sand	HS
1.11.10	39	147	Oolite	HS
1.11.10	40	147.75	Flakestone Breccia	HS
1.11.10	41	149.25	Flakestone Breccia	HS
1.11.10	42	150	Shale	HS
1.11.10	43	151.5	Shale	HS
1.11.10	44	153	Shale	HS
1.11.10	45	153	Shale	HS
1.11.10	46	154.5	Shale	HS
1.11.10	49	161.25	Carb. Cemented Fine Sand	HS
1.11.10	50	162.75	Carb. Cemented Fine Sand	HS
1.11.10	51	163.5	Flakestone Breccia	HS
1.11.10	52	163.5	Flakestone Breccia	HS
1.11.10	53	165	Flakestone Breccia	HS
1.11.10	54	165.75	Flakestone Breccia	HS
1.11.10	56	166.5	Flakestone Breccia	HS
1.11.10	57	168	Flakestone Breccia	HS
1.11.10	59	184.5	Flakestone Breccia	HS
1.11.10	60	195	Flakestone Breccia	HS
1.11.10	62	202.5	Marl	HS
1.11.10	63	203.25	Marl	HS
1.11.10	64	204	Marl	HS
1.11.10	66	210	Flakestone Breccia	HS
1.11.10	69	213	Stromatolite	HS
1.11.10	72	214.5	Stromatolite	HS
1.11.10	74	214.5	Carb. Cemented Fine Sand	HS
1.11.10	75	214.5	Shale	HS
1.11.10	77	216	Stromatolite	HS
1.11.10	80	216	Stromatolite	HS
1.11.10	81	216.75	Stromatolite	HS
1.11.10	83	217.5	Stromatolite	HS
1.11.10	85	219	Stromatolite	HS
1.11.10	87	222	Stromatolite	HS
1.11.10	88	222.75	Stromatolite	HS

Sample Series	Sample #	Stratigraphic Height (m)	Rock Type	Analysis
1.11.10	90	223.5	Stromatolite	HS
1.11.10	91	224.25	Stromatolite	HS
1.11.10	92	226.5	Stromatolite	HS
1.11.10	93	228	Stromatolite	HS
1.11.10	94	228.75	Stromatolite	HS
1.11.10	95	229.5	Stromatolite	HS
1.11.10	96	231	Stromatolite	HS
1.11.10	97	232.5	Stromatolite	HS

1.2 Trezona Range

Sample Series	Sample #	Stratigraphic Height (m)	Rock Type	Analysis
26.4.11	1	1	Shale Concretion	HS
26.4.11	2	2	Shale Concretion	HS, TS
26.4.11	3	3	Flakestone Breccia	HS
26.4.11	4	8	Flakestone Breccia	HS
26.4.11	5	10	Marl	HS
26.4.11	6	11	Flakestone Breccia	HS
26.4.11	7	12	Flakestone Breccia	HS, TS
26.4.11	8	13	Shale Concretion	HS
26.4.11	9	14	Shale Concretion	HS
26.4.11	10	15	Flakestone Breccia	HS
26.4.11	11	20	Shale Concretion	HS
26.4.11	12	16	Shale Concretion	HS
26.4.11	13	31	Carb. Cemented Fine Sand	HS
26.4.11	14	31	Flakestone Breccia	HS
26.4.11	15	31	Stromatolite	HS, TS
26.4.11	16	28	Flakestone Breccia	HS, TS
26.4.11	17	36	Carb. Cemented Fine Sand	HS
26.4.11	18	41	Stromatolite	HS
26.4.11	19	53	Flakestone Breccia	HS
26.4.11	20	54	Carb. Cemented Fine Sand	HS, TS
26.4.11	21	55	Stromatolite	HS
26.4.11	22	55	Marl	HS
26.4.11	23	57	Flakestone Breccia	HS
26.4.11	24	57	Flakestone Breccia	HS, TS
26.4.11	25	58	Carb. Cemented Fine Sand	HS, TS
26.4.11	26	61	Flakestone Breccia	HS
26.4.11	27	61	Flakestone Breccia	HS
26.4.11	28	68	Carb. Cemented Fine Sand	HS
26.4.11	29	69	Shale	HS
26.4.11	30	73	Flakestone Breccia	HS, TS
26.4.11	31	74	Flakestone Breccia	HS
26.4.11	32	89	Flakestone Breccia	HS, TS

26.4.11	33	90	Flakestone Breccia	HS
26.4.11	34	93	Flakestone Breccia	HS
26.4.11	35	93	Flakestone Breccia	HS
26.4.11	36	101	Shale	HS
26.4.11	37	110	Flakestone Breccia	HS
26.4.11	38	109	Stromatolite	HS
26.4.11	39	111	Oolite	HS, TS
26.4.11	40	125	Carb. Cemented Fine Sand	HS
26.4.11	41	131	Algal Laminite	HS
26.4.11	42	136	Algal Laminite	HS
26.4.11	43	140	Intraclastic Grainstone	HS
26.4.11	44	142	Intraclastic Grainstone	HS, TS
26.4.11	45	153	Intraclastic Grainstone	HS
26.4.11	46	155	Intraclastic Grainstone	HS
26.4.11	47	159	Intraclastic Grainstone	HS
26.4.11	48	163	Intraclastic Grainstone	HS
26.4.11	49	173	Intraclastic Grainstone	HS
26.4.11	50	179	Intraclastic Grainstone	HS
26.4.11	51	183	Intraclastic Grainstone	HS
26.4.11	52	185	Intraclastic Grainstone	HS
26.4.11	53	186	Intraclastic Grainstone	HS
26.4.11	54	197	Intraclastic Grainstone	HS
26.4.11	55	198	Stromatolite	HS
26.4.11	56	201	Intraclastic Grainstone	HS
26.4.11	57	203	Carb. Cemented Fine Sand	HS
26.4.11	58	210	Algal Laminite	HS
27.4.11	59	211	Algal Laminite	HS
27.4.11	60	212	Algal Laminite	HS
27.4.11	61	213	Algal Laminite	HS
27.4.11	62	221	Oolite	HS
27.4.11	63	222	Oolite	HS, TS
27.4.11	64	234	Algal Laminite	HS
27.4.11	65	235	Intraclastic Grainstone	HS, TS
27.4.11	66	237	Stromatolite	HS
27.4.11	67	238	Carb. Cemented Fine Sand	HS
27.4.11	68	240	Algal Laminite	HS
27.4.11	70	251	Flakestone Breccia	HS
27.4.11	71	251.5	Algal Laminite	HS
27.4.11	72	252	Flakestone Breccia	HS
27.4.11	73	257	Algal Laminite	HS
27.4.11	74	259	Algal Laminite	HS
27.4.11	75	260	Intraclastic Grainstone	HS
27.4.11	76	263	Algal Laminite	HS, TS
27.4.11	77	283	Intraclastic Grainstone	HS

27.4.11	78	284	Stromatolite	HS
27.4.11	79	285	Intraclastic Grainstone	HS
27.4.11	80	288	Intraclastic Grainstone	HS
27.4.11	81	294	Intraclastic Grainstone	HS, TS
27.4.11	82	291	Intraclastic Grainstone	HS
27.4.11	83	295	Intraclastic Grainstone	HS, TS
27.4.11	84	297	Stromatolite	HS, TS
27.4.11	85	303	Oolite	HS
27.4.11	86	305	Oolite	HS, TS
27.4.11	87	307	Stromatolite	HS
27.4.11	88	312	Algal Laminite	HS
27.4.11	89	313	Intraclastic Grainstone	HS, TS
27.4.11	90	322	Intraclastic Grainstone	HS
27.4.11	91	327	Stromatolite	HS
27.4.11	92	330	Stromatolite	HS
27.4.11	93	333	Intraclastic Grainstone	HS
27.4.11	94	336	Stromatolite	HS
27.4.11	95	339	Oolite	HS
27.4.11	96	341	Stromatolite	HS
27.4.11	97	344	Intraclastic Grainstone	HS, TS
27.4.11	98	345	Stromatolite	HS
27.4.11	99	349	Stromatolite	HS
27.4.11	100	350	Intraclastic Grainstone	HS
27.4.11	101	352	Stromatolite	HS

1.3 Little Bunkers Range

Sample Series	Sample #	Stratigraphic Height (m)	Lithology	Analysis
29.4.11	1	1	Shale	HS
29.4.11	2	2	Shale	HS
29.4.11	3	7	Flakestone Breccia	HS
29.4.11	4	24	Oolite	HS, TS
29.4.11	5	36	Flakestone Breccia	HS
29.4.11	6	38	Shale	HS
29.4.11	7	39	Flakestone Breccia	HS
29.4.11	8	39.5	Shale	HS
29.4.11	9	40	Flakestone Breccia	HS
29.4.11	10	41	Stromatolite	HS
29.4.11	11	41	Marl	HS
29.4.11	12	42	Stromatolite	HS
29.4.11	13	42	Stromatolite	HS
29.4.11	14	42.5	Stromatolite	HS
29.4.11	15	44	Flakestone Breccia	HS
29.4.11	16	45	Flakestone Breccia	HS

Date	No.	Depth	Lithology	Samples
29.4.11	17	46	Flakestone Breccia	HS, TS
29.4.11	18	46.5	Carb. Cemented Fine Sand	HS
29.4.11	19	47	Flakestone Breccia	HS
29.4.11	20	47.25	Flakestone Breccia	HS
29.4.11	21	47.5	Flakestone Breccia	HS
29.4.11	22	47.75	Flakestone Breccia	HS
29.4.11	23	48	Flakestone Breccia	HS, TS
29.4.11	24	49	Marl	HS
29.4.11	25	50	Carb. Cemented Fine Sand	HS
29.4.11	26	52	Carb. Cemented Fine Sand	HS
29.4.11	27	54	Flakestone Breccia	HS
29.4.11	28		Carb. Cemented Fine Sand	HS
29.4.11	29	55	Flakestone Breccia	HS
29.4.11	30	58	Flakestone Breccia	HS
29.4.11	31	59	Flakestone Breccia	HS
29.4.11	32	60	Flakestone Breccia	HS
29.4.11	33	61	Flakestone Breccia	HS
29.4.11	34	63	Carb. Cemented Fine Sand	HS
29.4.11	35	64	Flakestone Breccia	HS
29.4.11	36	65	Flakestone Breccia	HS
29.4.11	37	67	Carb. Cemented Fine Sand	HS
29.4.11	38	67.5	Carb. Cemented Fine Sand	HS
29.4.11	39	68	Flakestone Breccia	HS
29.4.11	40	69	Carb. Cemented Fine Sand	HS
29.4.11	41	104	Flakestone Breccia	HS
29.4.11	42	105	Shale	HS
29.4.11	43	106	Flakestone Breccia	HS
29.4.11	44	108	Flakestone Breccia	HS
29.4.11	45	109	Marl	HS
29.4.11	46	109.5	Flakestone Breccia	HS
29.4.11	47	110	Flakestone Breccia	HS
29.4.11	48	111	Flakestone Breccia	HS
29.4.11	49	117	Flakestone Breccia	HS
29.4.11	50	118	Carb. Cemented Fine Sand	HS
29.4.11	51	119	Flakestone Breccia	HS
29.4.11	52	120	Flakestone Breccia	HS
29.4.11	53	122	Flakestone Breccia	HS
29.4.11	54	123	Flakestone Breccia	HS
29.4.11	55	131	Carb. Cemented Fine Sand	HS
29.4.11	56	134	Flakestone Breccia	HS
29.4.11	57	135	Carb. Cemented Fine Sand	HS
29.4.11	58	136	Marl	HS
29.4.11	59	137	Marl	HS
30.4.11	1	138	Oolite	HS

30.4.11	2	138	Marl	HS
30.4.11	3	138.25	Oolite	HS
30.4.11	4	138.25	Oolite	HS, TS
30.4.11	5	138.5	Oolite	HS
30.4.11	6	138.5	Marl	HS
30.4.11	7	138.75	Intraclastic Grainstone	HS
30.4.11	8	138.75	Marl	HS
30.4.11	9	139	Intraclastic Grainstone	HS
30.4.11	10	139	Intraclastic Grainstone	HS
30.4.11	11	139.25	Marl	HS
30.4.11	12	139.25	Intraclastic Grainstone	HS
30.4.11	13	139.5	Marl	HS
30.4.11	14	139.5	Intraclastic Grainstone	HS
30.4.11	15	139.75	Marl	HS
30.4.11	16	139.75	Intraclastic Grainstone	HS
30.4.11	17	140	Marl	HS
30.4.11	18	140	Marl	HS
30.4.11	19	140.25	Marl	HS
30.4.11	20	140.25	Intraclastic Grainstone	HS
30.4.11	21	140.5	Marl	HS
30.4.11	22	140.5	Intraclastic Grainstone	HS
30.4.11	23	140.75	Marl	HS
30.4.11	24	140.75	Intraclastic Grainstone	HS
30.4.11	25	141	Marl	HS
30.4.11	26	141	Intraclastic Grainstone	HS
30.4.11	27	141.25	Marl	HS
30.4.11	28	141.25	Intraclastic Grainstone	HS
30.4.11	29	141.5	Marl	HS
30.4.11	30	141.5	Intraclastic Grainstone	HS
30.4.11	31	141.75	Marl	HS
30.4.11	32	141.75	Intraclastic Grainstone	HS
30.4.11	33	142	Intraclastic Grainstone	HS
30.4.11	34	142	Marl	HS
30.4.11	35	142.25	Intraclastic Grainstone	HS, TS
30.4.11	36	142.25	Marl	HS
30.4.11	37	142.5	Intraclastic Grainstone	HS
30.4.11	38	142.5	Marl	HS
30.4.11	39	143	Intraclastic Grainstone	HS
30.4.11	40	147	Intraclastic Grainstone	HS
30.4.11	41	148	Flakestone Breccia	HS
30.4.11	42	151	Carb. Cemented Fine Sand	HS, TS
30.4.11	43	153	Carb. Cemented Fine Sand	HS
30.4.11	44	153	Flakestone Breccia	HS
30.4.11	45	154	Carb. Cemented Fine Sand	HS

30.4.11	46	156	Shale	HS
30.4.11	47	157	Stromatolite	HS, TS
30.4.11	48	158	Intraclastic Grainstone	HS
30.4.11	49	159	Carb. Cemented Fine Sand	HS
30.4.11	50	160	Stromatolite	HS
30.4.11	51	163	Flakestone Breccia	HS
30.4.11	52	164	Intraclastic Grainstone	HS
30.4.11	53	165	Carb. Cemented Fine Sand	HS, TS
30.4.11	54	166	Stromatolite	HS
30.4.11	55	168	Oolite	HS, TS
30.4.11	56	170	Oolite	HS, TS
30.4.11	57	172	Stromatolite	HS, TS
30.4.11	58	174	Oolite	HS
30.4.11	59	177	Oolite	HS, TS
30.4.11	60	178	Oolite	HS
30.4.11	61	179	Oolite	HS
30.4.11	62	181	Oolite	HS
30.4.11	63	183	Oolite	HS, TS
30.4.11	64	184	Oolite	HS
30.4.11	65	186	Oolite	HS
30.4.11	66	189	Algal Laminite	HS
30.4.11	67	192	Oolite	HS
30.4.11	68	195	Oolite	HS, TS
30.4.11	69	198	Oolite	HS
30.4.11	70	204	Oolite	HS
30.4.11	71	208	Algal Laminite	HS
30.4.11	72	209	Oolite	HS, TS
30.4.11	73	214	Oolite	HS, TS
30.4.11	74	210	Oolite	HS
30.4.11	75	216	Oolite	HS
30.4.11	76	220	Oolite	HS
30.4.11	77	223	Oolite	HS
30.4.11	78	225	Stromatolite	HS
30.4.11	79	227	Stromatolite	HS
30.4.11	80	230	Stromatolite	HS
30.4.11	81	232	Stromatolite	HS
30.4.11	82	235	Stromatolite	HS
30.4.11	83	238	Stromatolite	HS
30.4.11	84	240	Stromatolite	HS
30.4.11	85	243	Stromatolite	HS
30.4.11	86	247	Stromatolite	HS
30.4.11	87	250	Oolite	HS
30.4.11	88	251	Oolite	HS
30.4.11	89	252	Stromatolite	HS

30.4.11	90	254	Stromatolite	HS
30.4.11	91	256	Oolite	HS
30.4.11	92	257	Oolite	HS, TS
1.5.11	1	264	Algal Laminite	HS, TS
1.5.11	2	264.5	Intraclastic Grainstone	HS
1.5.11	3	267	Intraclastic Grainstone	HS
1.5.11	4	270	Intraclastic Grainstone	HS
1.5.11	5	271	Intraclastic Grainstone	HS
1.5.11	6	271.25	Intraclastic Grainstone	HS
1.5.11	7	271.5	Intraclastic Grainstone	HS, TS
1.5.11	8	271.75	Marl	HS
1.5.11	9	272	Intraclastic Grainstone	HS
1.5.11	10	272.25	Marl	HS
1.5.11	11	272.5	Intraclastic Grainstone	HS
1.5.11	12	272.5	Intraclastic Grainstone	HS
1.5.11	13	272.75	Marl	HS
1.5.11	14	272.75	Intraclastic Grainstone	HS
1.5.11	15	273	Marl	HS
1.5.11	16	273	Intraclastic Grainstone	HS
1.5.11	17	273.25	Marl	HS
1.5.11	18	273.25	Intraclastic Grainstone	HS
1.5.11	19	273.5	Marl	HS
1.5.11	20	273.75	Intraclastic Grainstone	HS, TS
1.5.11	21	273.75	Intraclastic Grainstone	HS
1.5.11	22	274	Intraclastic Grainstone	HS
1.5.11	23	274.25	Intraclastic Grainstone	HS
1.5.11	24	274.5	Stromatolite	HS, TS
1.5.11	25	274.5	Intraclastic Grainstone	HS
1.5.11	26	274.75	Stromatolite	HS
1.5.11	27	274.75	Intraclastic Grainstone	HS
1.5.11	28	275	Intraclastic Grainstone	HS, TS
1.5.11	29	278	Algal Laminite	HS
1.5.11	30	280	Algal Laminite	HS
1.5.11	31	282	Stromatolite	HS
1.5.11	32	285	Stromatolite	HS
1.5.11	33	286	Stromatolite	HS
1.5.11	34	292	Stromatolite	HS
1.5.11	35	295	Stromatolite	HS
1.5.11	36	300	Algal Laminite	HS
1.5.11	37	306	Algal Laminite	HS
1.5.11	38	315	Algal Laminite	HS
1.5.11	39	324	Algal Laminite	HS
1.5.11	40	330	Carb. Cemented Fine Sand	HS
1.5.11	41	331	Algal Laminite	HS

1.5.11	42	336	Algal Laminite	HS
1.5.11	43	339	Algal Laminite	HS
1.5.11	44	343	Algal Laminite	HS
1.5.11	45	345	Algal Laminite	HS
1.5.11	46	348	Algal Laminite	HS
1.5.11	47	350	Carb. Cemented Fine Sand	HS
1.5.11	48	351	Carb. Cemented Fine Sand	HS

2.1 Blinman

Sample #	d13C (meas)	d18O (meas)	d13C Var.	d18O Var	d13C PDB	d18O PDB	cc 13-C	cc 18-O	Strat Height (m)
31.10.10.3	-7.0	-13.2	0.0	0.0	-7.0	-13.2			66
31.10.10.4a	-7.7	-14.0	0.0	0.0	-7.7	-14.0			66.5
31.10.10.4b	-7.7	-13.2	0.0	0.0	-7.7	-13.1			66.5
31.10.10.5	-7.6	-14.0	0.0	0.0	-7.6	-14.0			67
31.10.10.6	-7.9	-14.0	0.0	0.0	-7.9	-14.0			68
31.10.10.7	-7.7	-13.9	0.0	0.0	-7.7	-13.9			69
31.10.10.8	-7.8	-14.0	0.0	0.0	-7.8	-14.0			70
31.10.10.12	-5.9	-12.3	0.0	0.0	-5.9	-12.2			48
31.10.10.14	-8.1	-14.0	0.0	0.0	-8.1	-13.9			76
31.10.10.15	-8.3	-14.0	0.0	0.0	-8.3	-13.9			77
31.10.10.17	-8.4	-14.2	0.0	0.0	-8.4	-14.1			78
31.10.10.18	-8.3	-14.1	0.0	0.0	-8.2	-14.0			79
31.10.10.19	-8.3	-13.9	0.0	0.0	-8.2	-13.9			80
31.10.10.20	-7.9	-13.8	0.0	0.1	-7.8	-13.8			80.5
31.10.10.21	-7.6	-13.4	0.0	0.0	-7.5	-13.3			81
31.10.10.22	-8.3	-14.1	0.1	0.0	-8.2	-14.1			81.25
31.10.10.23	-8.3	-14.2	0.0	0.0	-8.3	-14.2			81.5
1-11-10 1A	-8.4	-13.0	0.1	0.1	-8.4	-13.0	**-8.5**	**-13.0**	115.5
1-11-10 1B	-8.6	-13.3	0.0	0.0	-8.6	-13.3	**-8.7**	**-13.3**	115.5
1-11-10 1C	-8.6	-13.5	0.1	0.0	-8.6	-13.5	**-8.7**	**-13.5**	115.5
1-11-10 2	-8.3	-12.5	0.0	0.0	-8.3	-12.5	**-8.3**	**-12.4**	116.25
1-11-10 3	-8.7	-13.0	0.1	0.1	-8.7	-13.0	**-8.7**	**-13.0**	117
1-11-10 4A	-8.5	-12.8	0.1	0.1	-8.5	-12.8	**-8.6**	**-12.8**	117.75
1-11-10 4B	-8.2	-12.8	0.0	0.1	-8.2	-12.8	**-8.3**	**-12.7**	117.75
1-11-10 5	-8.4	-13.2	0.1	0.1	-8.4	-13.2	**-8.5**	**-13.2**	117.75

1-11-10 6	-8.2	-12.4	0.2	0.2	-8.2	-12.4	**-8.3**	**-12.3**	118.5
1-11-10 7	-9.1	-12.7	0.1	0.1	-9.1	-12.7	**-9.2**	**-12.7**	118.5
1-11-10 8	-8.7	-12.8	0.1	0.2	-8.7	-12.8	**-8.8**	**-12.7**	119.25
1-11-10 9	-5.0	-7.6	0.2	0.2	-5.0	-7.6	**-5.0**	**-7.4**	120
1-11-10 10	-7.9	-11.7	0.1	0.1	-7.9	-11.7	**-8.0**	**-11.6**	120
1-11-10 11	-4.1	-5.0	0.2	0.2	-4.1	-5.0	**-4.1**	**-4.8**	120
1-11-10 12	-4.8	-3.7	0.1	0.2	-4.8	-3.7	**-4.8**	**-3.4**	121.5
1-11-10 12 (D)	-4.7	-4.0	0.2	0.2	-4.7	-4.0	**-4.7**	**-3.6**	121.5
1-11-10 13	-6.7	-4.8	0.0	0.0	-6.7	-4.8	**-6.7**	**-4.5**	121.5
1-11-10 14	-3.1	-4.6	0.2	0.2	-3.1	-4.6	**-3.1**	**-4.3**	122.25
1-11-10 15	-5.8	-10.0	0.0	0.0	-5.8	-10.0	**-5.8**	**-9.9**	123
1-11-10 16	-3.8	-5.1	0.2	0.2	-3.8	-5.1	**-3.8**	**-4.8**	123.75
1-11-10 17A	-7.7	-12.1	0.1	0.1	-7.7	-12.1	**-7.8**	**-12.1**	126
1-11-10 17B	-9.0	-13.2	0.0	0.1	-9.0	-13.2	**-9.0**	**-13.2**	126
1-11-10 18	-8.4	-13.3	0.0	0.0	-8.4	-13.3	**-8.5**	**-13.3**	126
1-11-10 19	-8.3	-11.7	0.1	0.1	-8.3	-11.7	**-8.4**	**-11.7**	126.75
1-11-10 20A	-8.3	-12.8	0.0	0.1	-8.3	-12.8	**-8.4**	**-12.8**	126.75
1-11-10 20B	-8.4	-13.4	0.1	0.0	-8.4	-13.4	**-8.5**	**-13.4**	126.75
1-11-10 21	-8.5	-13.1	0.1	0.1	-8.5	-13.1	**-8.6**	**-13.1**	127.5
1-11-10 22A	-8.3	-13.0	0.0	0.0	-8.3	-13.0	**-8.4**	**-13.0**	129
1-11-10 22B	-8.4	-12.4	0.1	0.1	-8.4	-12.4	**-8.4**	**-12.3**	129
1-11-10 23	-5.9	-8.5	0.1	0.1	-5.9	-8.5	**-5.9**	**-8.3**	133.5
1-11-10 24	-5.4	-8.1	0.1	0.1	-5.4	-8.1	**-5.5**	**-7.9**	133.5
1-11-10 25A	-8.3	-12.9	0.0	0.0	-8.3	-12.9	**-8.4**	**-12.9**	133.5
1-11-10 25B	-8.6	-13.8	0.0	0.0	-8.6	-14.0	**-8.8**	**-14.3**	134.25
1-11-10 26B	-7.9	-16.3	0.0	0.1	-7.9	-16.3	**-7.9**	**-16.4**	134.25
1-11-10 27	-9.5	-13.2	0.1	0.1	-9.5	-13.2	**-9.6**	**-13.2**	135
1-11-10 28	-9.1	-12.8	0.1	0.1	-9.1	-12.8	**-9.2**	**-12.8**	136.5

1-11-10 29	-8.4	-12.3	0.1	0.1	-8.4	-12.3	**-8.5**	**-12.3**	136.5
1-11-10 30	-8.4	-13.2	0.1	0.1	-8.4	-13.2	**-8.5**	**-13.2**	138
1-11-10 31	-8.5	-13.5	0.0	0.0	-8.5	-13.5	**-8.6**	**-13.5**	139.5
1-11-10 32	-8.3	-12.4	0.2	0.1	-8.3	-12.4	**-8.3**	**-12.4**	139.5
1-11-10 33	-8.3	-13.3	0.1	0.1	-8.3	-13.3	**-8.4**	**-13.3**	139.5
1-11-10 34	-8.1	-11.7	0.1	0.1	-8.1	-11.7	**-8.1**	**-11.7**	141
1-11-10 37 (B)	-8.5	-12.5	0.1	0.1	-8.5	-12.5	**-8.6**	**-12.5**	145.5
1-11-10 38	-8.7	-13.0	0.1	0.2	-8.7	-13.0	**-8.8**	**-13.0**	147
1-11-10 39A (B)	-8.7	-12.7	0.1	0.1	-8.7	-12.7	**-8.8**	**-12.7**	147
1-11-10 39B (B)	-8.3	-12.5	0.1	0.1	-8.3	-12.5	**-8.4**	**-12.5**	147
1-11-10 40B	-8.5	-10.4	0.0	0.1	-8.5	-10.4	**-8.6**	**-10.3**	147.75
1-11-10 40C (B)	-8.6	-11.2	0.1	0.1	-8.6	-11.2	**-8.7**	**-11.1**	147.75
1-11-10 41 (B)	-9.5	-13.1	0.1	0.1	-9.5	-13.1	**-9.6**	**-13.1**	149.25
1-11-10 42 (B)	-9.9	-13.1	0.1	0.1	-9.9	-13.1	**-10.0**	**-13.1**	150
1-11-10 43 (B)	-10.7	-12.9	0.1	0.1	-10.7	-12.9	**-10.8**	**-12.9**	151.5
1-11-10 44 (B)	-6.2	-9.2	0.2	0.2	-6.2	-9.2	**-6.2**	**-9.1**	153
1-11-10 45 (B)	-10.0	-13.1	0.1	0.1	-10.0	-13.1	**-10.3**	**-13.4**	153
1-11-10 46 (B)	-8.4	-11.7	0.1	0.2	-8.4	-11.8	**-8.6**	**-12.0**	154.5
1-11-10 49 (B)	-9.0	-11.4	0.0	0.0	-9.0	-11.4	**-9.1**	**-11.3**	161.25
1-11-10 50 (B)	-8.6	-12.8	0.0	0.0	-8.6	-12.8	**-8.7**	**-12.8**	162.75
1-11-10 51 (B)	-8.9	-14.1	0.0	0.1	-8.9	-14.2	**-9.1**	**-14.5**	163.5
1-11-10 52 (B)	-8.8	-12.5	0.1	0.1	-8.8	-12.6	**-9.0**	**-12.9**	163.5
1-11-10 53 (B)	-8.7	-13.1	0.0	0.0	-8.7	-13.3	**-8.9**	**-13.6**	165
1-11-10 54 (B)	-8.8	-13.5	0.1	0.1	-8.8	-13.5	**-8.8**	**-13.5**	165.75
1-11-10 56 (B)	-8.5	-12.5	0.0	0.0	-8.5	-12.6	**-8.7**	**-12.8**	166.5
1-11-10 57 (B)	-8.7	-13.0	0.1	0.1	-8.7	-13.1	**-8.9**	**-13.4**	168
1-11-10 59 (B)	-8.7	-14.1	0.1	0.1	-8.7	-14.1	**-8.8**	**-14.2**	184.5
1-11-10 59B (B)	-8.3	-12.9	0.0	0.0	-8.3	-12.9	**-8.3**	**-12.9**	184.5

1-11-10 60 (B)	-8.3	-12.8	0.1	0.1	-8.3	-12.8	**-8.4**	**-12.8**	195
1-11-10 62 A (B)	-8.5	-13.2	0.1	0.1	-8.5	-13.4	**-8.7**	**-13.6**	202.5
1-11-10 62 B (B)	-8.4	-13.2	0.1	0.1	-8.4	-13.3	**-8.6**	**-13.6**	202.5
1-11-10 63 (B)	-8.0	-13.4	0.1	0.1	-8.0	-13.4	**-8.1**	**-13.4**	203.25
1-11-10 64 (B)	-8.3	-14.8	0.0	0.0	-8.3	-14.8	**-8.4**	**-14.8**	204
1-11-10 66A (B)	-7.3	-17.9	0.0	0.0	-7.3	-18.0	**-7.5**	**-18.5**	210
1-11-10 66B (B)	-7.8	-16.7	0.1	0.1	-7.8	-16.8	**-8.0**	**-17.2**	210
1-11-10 69 A (B)	-8.2	-13.1	0.1	0.0	-8.2	-13.3	**-8.4**	**-13.5**	213
1-11-10 72 (B)	-8.1	-13.4	0.1	0.1	-8.1	-13.5	**-8.3**	**-13.7**	214.5
1-11-10 74 (B)	-8.1	-12.8	0.1	0.1	-8.1	-12.9	**-8.3**	**-13.2**	214.5
1-11-10 75 (B)	-7.5	-11.8	0.0	0.0	-7.5	-11.9	**-7.7**	**-12.1**	214.5
1-11-10 77 (B)	-7.7	-13.9	0.0	0.0	-7.7	-14.1	**-7.8**	**-14.4**	216
1-11-10 80 (B)	-8.0	-13.0	0.0	0.1	-8.0	-13.1	**-8.1**	**-13.4**	216
1-11-10 81 (B)	-7.6	-12.0	0.1	0.1	-7.6	-12.0	**-7.6**	**-11.9**	216.75
1-11-10 83 (B)	-7.6	-13.3	0.0	0.1	-7.6	-13.4	**-7.7**	**-13.7**	217.5
1-11-10 85 (B)	-7.2	-12.5	0.1	0.0	-7.2	-12.5	**-7.2**	**-12.5**	219
1-11-10 87 (B)	-7.4	-13.2	0.1	0.1	-7.4	-13.3	**-7.6**	**-13.6**	222
1-11-10 88 (B)	-6.6	-11.7	0.0	0.0	-6.6	-11.7	**-6.7**	**-11.7**	222.75
1-11-10 90 (B)	-6.9	-13.0	0.1	0.0	-6.9	-13.0	**-6.9**	**-13.0**	223.5
1-11-10 91 (B)	-7.1	-12.7	0.0	0.0	-7.1	-12.7	**-7.2**	**-12.7**	224.25
1-11-10 92 (B)	-6.3	-12.9	0.0	0.1	-6.3	-12.9	**-6.3**	**-12.9**	226.5
1-11-10 93	-4.6	-13.1	0.0	0.0	-4.6	-13.1	**-4.7**	**-13.1**	228
1-11-10 94 (B)	-3.8	-13.2	0.1	0.1	-3.8	-13.2	**-3.8**	**-13.2**	228.75
1-11-10 95 (B)	-3.1	-12.7	0.1	0.1	-3.1	-12.7	**-3.1**	**-12.6**	229.5
1-11-10 96	-4.8	-13.5	0.1	0.1	-4.8	-13.5	**-4.9**	**-13.5**	231
1-11-10 97	-1.4	-9.2	0.1	0.1	-1.4	-9.2	**-1.4**	**-9.0**	232.5

2.2 Emu Gap

Stratigraphic Height(m)	13C carb	18O carb	13C org	D 13C	TOC	Sample
0.3	-8.7	-13				limestone
0.5	-8.6	-12.6				limestone
12.3	-8.8	-12.5	-23.9	15.1	0.011	limestone
13.9	-8.7	-11.7				limestone
14.9	-8.6	-12.3				limestone
14.9	-8.5	-12.8				limestone
15.5	-8.5	-12.5				limestone
16.2	-8.4	-12.7				limestone
17.1	-8.6	-12.9				limestone
25	-8.6	-12.9	-26.4	17.7	0.005	limestone
27.4	-8.6	-12.4				limestone
34.1	-8.2	-12.6				limestone
34.5	-8.2	-12.6				limestone
34.8	-8.1	-12.6	-25.4	17.3	0.005	limestone
36.1	-8.6	-11.8				limestone
36.4	-8.7	-12.6				limestone
38.3	-9.5	-12.1	-24.4	14.9	0.016	limestone
46.5	-8.5	-12.8				limestone
47.7	-8.7	-12.1				limestone
48.3	-8.8	-12.6				limestone
54.8	-8.4	-11.8				limestone
55.9	-8.6	-12.2				limestone
56.2	-8.8	-11.2				limestone
56.2	-8.3	-12.2				limestone
56.3	-8.8	-12.5				limestone
57.7	-8.3	-12.4				limestone
59.4	-9	-11.9				limestone
61.7	-8.6	-12.1				limestone
63.4	-9.7	-12.3				limestone
63.8	-8.8	-12.2				limestone
64.9	-9.5	-11.9	-23.2	13.7	0.013	limestone
67.1	-8.6	-12.2				limestone
67.9	-8.5	-12.1				limestone
68.6	-8.8	-11.6				limestone
71.9	-8.1	-11.6	-23.9	15.8	0.013	limestone
72.9	-8.7	-12.1				limestone
73.3	-8.3	-12				limestone
74.5	-8.2	-12.2				limestone
75.3	-8.1	-11.8				limestone
76.5	-8.2	-12.2				limestone

77	-8.3	-12.1	-26.4	18.2	0.007	limestone
77.3	-8.5	-12.1				limestone
80.5	-8.3	-11.2				limestone
81.2	-8.9	-10.3				limestone
81.5	-8.8	-11.9				limestone
82.3	-8.9	-12	-27.5	18.6	0.012	limestone
82.6	-9.4	-11.7				limestone
87.3	-8.3	-11.7				limestone
89.4	-8.9	-11.5				limestone
91.5	-8.6	-11.3				limestone
93.7	-8.7	-11.9				limestone
94.6	-8.7	-11.9				limestone
97	-8.6	-11.9				limestone
98.2	-8.3	-11.7				limestone
99.2	-8.1	-11.7				limestone
100.1	-8.4	-11.8				limestone
100.7	-9.2	-11.4				limestone
101.4	-8.8	-11.3	-24.2	15.4	0.016	limestone
103.8	-9.6	-11.6				limestone
106.5	-8.1	-11.1				limestone
107.4	-7.9	-10.6				limestone
108.3	-8.5	-9.4				limestone
109	-9.8	-7.7	-24.3	14.6	0.009	limestone
117.8	-8.3	-11.4				limestone
118.4	-8.1	-10.8				limestone
122.4	-7.7	-11.3				limestone
124	-7.5	-11.3				limestone
124.8	-7.7	-11.2				limestone
125.8	-7.5	-10.9				limestone
126.6	-7.5	-9.5				limestone
127.1	-7.5	-8.9	-27.9	20.4	0.009	limestone
127.8	-7.7	-10.5				limestone
128.6	-7.4	-8.5				limestone
129.8	-7.6	-8.5				limestone
130.8	-7.9	-9.6				limestone
131.6	-8	-8.9				limestone
132.5	-7.7	-8.7				limestone
133.1	-7.7	-9.1				limestone
134.2	-7.7	-8.6				limestone
135.2	-7.4	-10.2				limestone
136	-7.6	-10.4				limestone
136.8	-7.6	-10.2				limestone
137	-7.6	-9.8	-24.9	17.3	0.006	limestone
138.1	-7.5	-9.1				limestone

138.6	-7.2	-10.2				limestone
139.6	-7.3	-10.2	-25	17.7	0.011	limestone
142.7	-7.4	-10				limestone
148.3	-7.7	-8.6	-30.1	22.5	0.014	limestone
149.5	-7.2	-9.9				limestone
150.2	-7.3	-9.9				limestone
152.2	-7.1	-9.2				limestone
153.8	-7.4	-8.8				limestone
155	-7.3	-8.6	-27	19.8	0.007	limestone
155.7	-7.4	-7.6				limestone
156.4	-7.3	-9.2				limestone
156.7	-6.8	-9.4				limestone
157.2	-6.8	-9.3				limestone
157.7	-6.7	-9.5				limestone
158.5	-6.7	-9.6				limestone
159.9	-6.6	-9.6	-24.8	18.3	0.008	limestone
160.5	-6.6	-9.5				limestone
161	-6.7	-9.3				limestone
162.3	-6.4	-9.6				limestone
162.9	-6.2	-9.6				limestone
165.7	-6.5	-9.5	-26	19.5	0.011	limestone
166.4	-6.5	-9.7				limestone
167.3	-6.4	-9.5				limestone
167.6	-6.3	-9.4				limestone
168.4	-6.9	-9.5	-26.5	19.5	0.009	limestone
169.8	-6.4	-9.5				limestone
170.5	-6.4	-9.4				limestone
171.4	-6.4	-9.6				limestone
172.4	-6.1	-9.4				limestone
173.1	-6.1	-9.6				limestone
174.1	-6.1	-9.5				limestone
175.1	-6.3	-9.7				limestone
175.3	-6	-9.6				limestone
175.4	-6.2	-9.5	-26.1	19.8	0.009	limestone
176.5	-6	-9.6				limestone
177.8	-6	-9.6				limestone
179	-5.8	-9.4				limestone
180.6	-5.9	-9.6				limestone
181	-5.9	-9.6				limestone
181.3	-5.7	-8.7				limestone
182.4	-5.9	-8.8				limestone
183.6	-5.8	-8.6				limestone
184.6	-6.2	-9.4	-23.7	17.5	0.013	limestone
185.3	-6.2	-9.6				limestone

186.3	-6.1	-9.4				limestone
187	-6.1	-9.5				limestone
188.4	-5.9	-9.5	-25.2	19.3	0.012	limestone
189.7	-5.7	-9.6				limestone
190.6	-5.5	-9.3				limestone
191.7	-5.6	-9.5				limestone
192.5	-5.8	-9.3				limestone
193	-5.9	-9.4				limestone
193.3	-5.9	-9.5	-25.2	19.3	0.009	limestone
194.1	-5.7	-9.6				limestone
195.1	-5.7	-8.1				limestone
196.8	-5.9	-9.3	-25.2	19.3	0.004	limestone
197.1	-5.5	-9.4				limestone
197.6	-5.5	-9.6				limestone
198.8	-5.5	-9.6				limestone
199.7	-5.4	-8.9				limestone
200.8	-5.5	-9.6	-24.8	19.2	0.007	limestone
201.7	-5.3	-9.4				limestone
201.9	-5.5	-9.1				limestone
203.1	-5.2	-9.1				limestone
204.1	-5.7	-8.7				limestone
205.1	-5.6	-8.9				limestone
206.6	-6.2	-8.2				limestone
206.7	-5.1	-9.1	-26.2	21.1	0.014	limestone
207.5	-5.4	-8.9	-25.7	20.3	0.009	limestone
208.5	-5.4	-8.9				limestone
209.6	-5.5	-9.3				limestone
211.1	-4.7	-9.5				limestone
212.1	-5	-10				limestone
212.8	-4.8	-9.6				limestone
213.5	-4.8	-9.9				limestone
214.2	-5.3	-9.6	-25.4	20.1	0.007	limestone
215.1	-4.8	-8.8				limestone
216.1	-5.3	-9.8				limestone
216.9	-5.3	-10				limestone
217.9	-5.1	-8.4	-23.5	18.4	0.011	limestone
219.8	-4.9	-9.8				limestone
221.1	-4.6	-9.7				limestone
222.5	-4.7	-10				limestone
223.5	-4.5	-9.9	-24	19.5	0.006	limestone
224.4	-5.2	-8.1				limestone
224.7	-4.5	-9.2	-25.6	19.3	0.005	limestone
224.9	-4.5	-8.3				limestone
226.9	-4.9	-8.6				limestone

228.1	-4.5	-9.5				limestone
228.8	-4.5	-9.4				limestone
229.3	-4.7	-9				limestone
231.1	-4.2	-9.6	-25.9	21.7	0.008	limestone
232.1	-4.7	-8.2				limestone
233.3	-4.1	-9.4				limestone
234	-4.1	-9.4				limestone
234.5	-4.2	-9.6				limestone
235.2	-4.2	-9.4				limestone
236.5	-4.1	-9.6	-24.9	20.9	0.008	limestone
237.5	-4.1	-9.9				limestone
238.6	-3.9	-9.4				limestone
239.7	-3.7	-9.3				limestone
241.1	-3.7	-9.3				limestone
242.3	-3.8	-10				limestone
243	-3.7	-10.1				limestone
243.9	-3.7	-10	-24.7	21	0.011	limestone
245	-3.6	-10				limestone
246	-3.6	-9.7				limestone
247.2	-3.7	-10.2				limestone
247.9	-3.5	-9.8				limestone
248.9	-3.6	-10.1	-24.5	20.9	0.009	limestone
249.9	-3.9	-9.8				limestone
250.9	-3.4	-9.3				limestone
251.9	-3.6	-10.4				limestone
252.9	-3.6	-10.2				limestone
254	-3.7	-10.2	-24.1	20.4	0.008	limestone
255	-4.3	-10.5				limestone
255.6	-3.4	-10.4	-23.5	20.1	0.008	limestone
256.7	-3.1	-10.4				limestone
257.5	-3.3	-10				limestone
258.4	-3.1	-10.1				limestone
259.6	-3.3	-10.2	-23.7	20.5	0.007	limestone
261	-3.5	-10.8				limestone
261.7	-2.9	-10.6				limestone
262.7	-3.1	-10.7				limestone
263.6	-3.5	-9.6				limestone
264.4	-3.4	-10.7	-25.7	22.4	0.017	limestone
265.2	-3.2	-10.6				limestone
266.2	-3.3	-10.6	-25.2	21.9	0.013	limestone
266.5	-3.3	-10.8				limestone
266.8	-3.3	-10.9				limestone
267.3	-3.3	-10.9				limestone
268.4	-3.4	-11				limestone

268.9	-3.6	-11.1				limestone
269.4	-3.8	-12.2				limestone
270.5	-3.4	-12.5	-24.8	22	0.018	limestone
271.4	-3.4	-12.6				limestone
271.6	-3.5	-12.7				limestone
300	-5	-9.6	-26.6	21.6	0.015	limestone

3.1 Trezona Range

Sample	Lithology	Petrographic descriptions
26.4.11.2	**Concreted Shale**	Matrix: Laminated silt, cement is ~10% of mass.
26.4.11.7	**Intraclastic Algal-Flake Breccia**	Matrix: Micritic and locally microspar (coarsens towards void space) Clasts: Micritic 3-15 mm long, 1-3 mm wide, rounded clasts (probably algal flakes). Darker than matrix due to insolubles on micrite crystal margins. Coarse, equant to bladed pseudospar (minor microspar) crystals replacing flake intraclast interiors. Where clast margin is breached, pseudospar crystals are sometimes continuous with matrix (and matrix penetrates clast). Space between pseudospar crystals is very dark due to the concentration of insoluble material (derived from the micritic clast that was replaced). Sedimentary Structure: Clasts occur roughly parallel to bedding plane. Clasts appear stacked suggesting storm-driven deposition. Diagenesis: Dissected by stylites that truncate micritic clasts and are truncated by pseusospar-replaced clasts. Suggests replacement precedes stylite dissolution. Matrix is likely recrystallised micrite that filled void space soon after deposition or is micrite recrystallised post-deposition from pore fluids.
26.4.11.15	**Stromatolite Mound**	Matrix: Micritic (calcite, pale pink stain) with lenses of pelitic sediment (usually silt with angular quartz) and quartz crystals throughout. Major sharp boundary (see photo) is likely an erosional surface where stromatolite was covered by a veneer of pelitic sediment. Cut by modern, millimetre-thick veins.
26.4.11.16	**Intraclastic Algal-Flake Breccia**	Matrix: Dominantly microspar with abundant quartz grains and insoluble material. Void space is dominantly filled with equant-tabular pseudospar crystals with insoluble-rich margins. Clasts: Elongate, rounded algal-flake clasts comprising micrite. Clast margins are not sharp but a distinct grain-size difference is visible. Occurs as a 'stacked' package of algal-flake clasts cemented by a pseudospar-microspar matrix. Different from 26.4.11.7 due to the abundance of pelitic and insoluble material occurring in intervening space between clasts. Dark layers, possibly silt, occur on one side of many of the intraclasts
26.4.11.20	**Red Fine Sand**	Carbonate cemented sand with micas (muscovite) and micritic layers. Cement-sand ratio is highly variable, base is more micritic, the majority of the sample is sand-dominated (and supported by sand grains). Cement is calcitic (stains pale pink-red)
26.4.11.24	**Intraclastic Grainstone**	Matrix: Micrite Clasts: A mixture of ~1cm long algal flakes (micritic) and micritic mud rip-ups, blebs and ooids. All clasts have micritic rims with the interiors recrystallised to microspar and pseudospar (with few rhombic carbonate crystals). Space between clasts, transitioning from matrix micrite, comprises coarse mosaics of spar (microspar to coarse pseudospar into void space). Internal sediment bounded by some clasts (and surrounding ooids and small blebs) comprises highly crushed and recrystallised material (look like pellets) mixed with quartz crystals and supported by micrite. A clast occurs with breached margins, void within clast is filled with internal sediment.

26.4.11.25	carbonate cemented sand	Micrite with a sand/mica 'channel' cut into it. Matrix: Micritic with vugs filled with microspar-pseudospar, coarsening towards void space. Clasts: Broadly micritic (as in 26.4.11.7), except the micrite coarsens to microspar towards the centre of each clast. Other clasts are more equant (blebs), both flake and bleb clasts also appear as equant microspar-pseudospar mosaics. All carbonate crystals concentrate insoluble material in their rims. Abundant crushed-clast fabrics are observed.
26.4.11.30	intraclastic grainstone	Matrix: Micritic with vugs filled with microspar-pseudospar, coarsening towards void space. Clasts: Broadly micritic (as in 26.4.11.7), except the micrite coarsens to microspar towards the centre of each clast. Other clasts are more equant (blebs), both flake and bleb clasts also appear as equant microspar-pseudospar mosaics. All carbonate crystals concentrate insoluble material in their rims. Abundant crushed-clast fabrics are observed.
26.4.11.32	Intraclastic Grainstone	Matrix: Dominantly microspar, but ranges from microspar to very coarse pseudospar. Clasts: Crushed algal flakes, ooids, mud rip-up clasts. Very highly recrystallised grainstone preserving crushed clasts of flake, ooid and bled morphologies. Clasts are, for the most part, only recognisable due to insoluble material at their margins. Spar morphology depends on clast interior. Few clasts with better texture preserve a transition from micrite to coarse microspar towards the clast interior.
26.4.11.39	Intraclastic Grainstone	Similar texture to 26.4.11.32 but more ooid-dominated. Less evidence of clasts from insoluble materials. A major quartz-rich structure passes through the sample, potentially a dissolution seam concentrating insoluble grains along its length.
27.4.11.44	Intraclastic Grainstone	Matrix: Micrite (unrecrystallised) and microspar (crystallised) Comprised of a relatively homogeneous massive micrite with a layer of highly crushed and dissolved material. The layer is likely a significant dissolution seam. The interior of the dissolution seam-bounded area comprises a dominantly micritic-microspar matrix supporting crushed clasts of algal flakes, blebs and ooids. Coarse pseudospar crystals often preserve the shape of recrystallised clasts (such as ooids, see photo). Seams also seem to preserve accumulations of quartz crystals and elongate pseusospar crystals (weird green stain), assumedly insoluble when the pressure solution event occurred. A lense of early, undamaged texture is preserved comprising algal flakes altering to microspar from micrite and microspar-replaced ooids, both with radial microspar margins. Mg-calcite is prevalent within the sample, dominantly in matrix microspar and on the margins of clasts.
27.4.11.63	Ooid dominated intraclastic grainstone	Matrix: Dominantly microspar, coarsens slightly toward space between clasts. Clasts: Micritic flake, bleb and ooid clasts as well as recrystallised clasts of these (where margins are breached, more microspar-pseudosparry). Clasts are coated with a grey micritic rim unlike the micrite preserved within grains, probably post-initial deposition. Lenses of clasts with 'elephantine' features occur, suggesting post-depositional deformation.
27.4.11.65	Intraclastic Grainstone	Matrix: Micrite-Microspar Clasts: Derived from other lithologies. Micrite algal flakes, laminated marl rounded-elongate clasts, ooid grainstone clasts. Clasts with breached margins appear to be recrystallised to coarse pseudospar.

27.4.11.76	Algal laminate	Matrix: Micritic with very sparse quartz grains. Layering defined by darker texture (probably silty) and uncommon bound quartz grains. Very pale red stain (calcite)
27.4.1.81	intraclastic Grainstone	Matrix: Microspar dominated Clasts: Few algal-flake clasts are identifiable (micrite-dominated). Sample is so recrystallised that more texture appears to be gone OR there were very few clasts to begin (massive marl).Vug-filling 'dog-tooth' crystals.
27.4.11.83	Intraclastic Grainstone	Matrix: Dominantly microspar, coarsens slightly toward space between clasts. Clasts: Micritic flake, bleb and ooid clasts as well as recrystallised clasts of these (where margins are breached, more microspar-pseudosparry). Clasts are coated with a grey micritic rim unlike the micrite preserved within grains, probably post-initial deposition. Lenses of clasts with 'elephantine' features occur, suggesting post-depositional deformation.
27.4.11.84	Stromatolite	Micritic stromatolite with pelitic horizons and bound quartz cryatals.
27.4.11.86	Ooid Grainstone	Matrix: Micritic on one side of stylite, microspar on the other. Clasts comprised entirely of ooids with micritic rims. Interiors are replaced with, usually singular but not always, spar crystals that preserve the ooid shape (but not internal texture). Micritic rims tend to not be dissolved (as seen in 27.83).
27.4.11.97	Intraclastic Grainstone	Matrix: Micrite-Microspar Clasts: Derived from other lithologies. Micrite algal flakes, laminated marl rounded-elongate clasts, ooid grainstone clasts. Clasts with breached margins appear to be recrystallised to coarse pseudospar.

3.2 Little Bunkers Range

Sample	Lithology	Petrographic descriptions
29.4.11.4	Ooid Grainstone	Matrix: Micrite to fine microspar. Micritic layers lacking ooids. Stained pale pink (calcite) Clasts: Recrystallised ooids with minor micritic algal flakes (no sparry flakes). Ooids are generally single spar crystals.
29.4.11.17		Matrix: Micrite with very fine quartz inclusions. Somewhat micaceous Clasts: fine, elongate 'lenses' of silty carbonate-cemented material. May be from finely laminated marls.
29.4.11.23	Carbonate cemented fine sand	Matrix supported, fe calcite. Micaceous
30.4.11.4	Intraclastic Grainstone	Matrix: Dominantly microspar mosaic with some micrite and pseudospar. Clasts: Algal flakes and ooids. Dominantly micritic with some internal recrystallization to pseudospar. All clasts preserve micritic rims.
30.4.11.35	Intraclastic Grainstone	Matrix: microspar to pseudospar, coarsening away from clasts (into void). No remaining micrite.
30.4.11.42	Carbonate cemented laminated sand (internally cross bedded)	Carbonate-dominated cemented fine sand. Micaceous (muscovite) with internal cross beds defined by more marly layers.
30.4.11.47	Stromatolite (calcite)	Matrix: Micrite with random clasts of fine sand incorporated. Layering defined by more silty horizons.
30.4.11.53	laminated fine sand (cemented)	

30.4.11.55	**Ooid Grainstone**	Matrix: Microspar Clasts: Ooids. Ooid clasts and matrix are microspar dominantly with some pseudospar crystal replacement of ooids (single crystals inside the ooid). Silty? layers separate two major ooid units, with an intermediate 1 cm marl layer. Suggests a break in ooid deposition due to sudden dep. environmental change (unlikely to be erosional). Grains of qtz that have fallen into the lime mud create void for microspar growth within the marl layer.
30.4.11.56	**Ooid Grainstone**	Matrix: Microspar Clasts: Microspar-Replaced ooids continuous with matrix. Only remnant of ooid shape in insoluble material rims. Highly dissected by stylites.
30.4.11.57	**Interbedded marl and pelitic (+musc) layers**	Matrix: Microspar Clasts: Microspar-Replaced ooids continuous with matrix. Only remnant of ooid shape in insoluble material rims. Highly dissected by stylites. Plus modern vein and big stylite.
30.4.11.59	**Ooid Grainstone**	Matrix: Microspar Clasts: Microspar-Replaced ooids continuous with matrix. Only remnant of ooid shape in insoluble material rims. Highly dissected by stylites.
30.4.11.63	**Ooid Grainstone**	Matrix: Micrite Clasts: v. highly recrystallised ooids with/without micritic rims. Qtz grain common. Some ooids are elongate (deformed). Cut by a dissolution seam vein thing filled with blocky pseudospar and marginally rich in qtz grains.
30.4.11.68	**Ooid Grainstone**	Matrix: Micrite with areas of microspar Clasts: Primarily pseudospar flake clasts, some miritic clasts. Distinct lack of ooids (very few). Similar to texture seen much earlier, suggests cyclicity? No ooids which is weird considering adjacent lithofacies.
30.4.11.72	**intraclastic Grainstone**	Micritic-microspar, layered laminate. Layer defined by very qtz and silt-rich horizons. Incorporates a clast surrounded by sand, which adorable.
30.4.11.73	**Algal Laminite**	Matrix: microspar Clasts: well-preserved ooids (singh texture with the segments) Ooids are micritic at their margins and coarsen up towards their centre. Central to most ooids is an accumulation of insoluble materials. Dissolution seams.
30.4.11.92	**Ooid Grainstone**	Matrix: Micrite Clasts: Pseudospar-replaced ooids. Usually one crystal per ooid. cross cut by modern veins
1.5.11.1	**Ooid grainstone**	Matrix: Micrite (Matrix supported) Clasts: Probably algal flakes, curled due to being matrix supported (probably). Dog-tooth microspar on margins of grains, which quickly coarsen up to very coarse pseudospar mosaic fills. Very few (usually much thinner) micrite-microspar flake clasts preserved.
1.5.11.7	**Intraclastic Grainstone**	Matrix: Micrite with abundant fine sand. Clasts: Probably algal flakes, curled due to being matrix supported (probably). Dog-tooth microspar on margins of grains, which quickly coarsen up to very coarse pseudospar mosaic fills. Very few (usually much thinner) micrite-microspar flake clasts preserved.
1.5.11.20	**intraclastic grainstone**	Micrite matrix with layering defined by silt.
1.5.11.24	**Stromatolite**	Matrix: micrite-minor microspar. Clasts: Some micritic flake-

		clasts and vugs filled with well-formed spar crystals (some rhomboid).
1.5.11.28	**Intraclastic Grainstone**	Matrix: Micrite. Clasts: Crushed, deformed flake clasts, some with minor micrite rims. Centimeter clasts of siltstone and fine sandstone are supported by matrix and flake mass. Some minor ooids with micritic rims.